Systematic study of bremsstrahlung emission in reactions with light nuclei in cluster models

S. P. Maydanyuk [1,2,*] and V. S. Vasilevsky [3,†]
[1] *Wigner Research Centre for Physics, Budapest 1121, Hungary*
[2] *Institute for Nuclear Research, National Academy of Sciences of Ukraine, Kyiv 03680, Ukraine*
[3] *Bogolyubov Institute for Theoretical Physics, Metrolohichna Street 14b, Kyiv 03143, Ukraine*

(Received 26 April 2023; accepted 23 October 2023; published 4 December 2023)

A new model of the bremsstrahlung emission in the scattering of light nuclei is constructed with the main focus on the strict cluster formulation for nuclear processes. The analysis is performed in the frameworks of the folding approximation for s nuclei. The reactions $p + {}^4\mathrm{He}$, ${}^2\mathrm{H} + {}^4\mathrm{He}$, ${}^3\mathrm{H} + {}^4\mathrm{He}$, and ${}^3\mathrm{He} + {}^4\mathrm{He}$ are considered. The properties of the emission of bremsstrahlung photons in a wide region of kinetic energies of relative motion of two nuclei from 7 to 1000 MeV are systematically studied. The influence of the oscillator length on the calculated bremsstrahlung emission spectra is discussed. Using the example of ${}^3\mathrm{H} + {}^4\mathrm{He}$, the dependence of the bremsstrahlung spectra on parameters of the nuclear component of the interaction potential is established (for the first time for light nuclei). Experimental bremsstrahlung data for the proton-deuteron scattering and proton–α-particle scattering are described on the basis of this model.

DOI: 10.1103/PhysRevC.108.064001

I. INTRODUCTION

The bremsstrahlung emission of photons accompanying nuclear reactions is an important topic of nuclear physics and has attracted significant interest of many researchers for a long time (see reviews [1–4]). This is explained by the fact that the spectra of bremsstrahlung photons are calculated on the basis of nuclear models with include mechanisms of reactions, interactions between nuclei, dynamics, and many other physical issues. The measurements of those photons and their analysis provide the information about all these aspects, by verifying the suitability of the developed models.

Investigations of the bremsstrahlung emission in proton-nucleus scattering have shown the important role of incoherent bremsstrahlung processes. In particular, in Refs. [5,6] (see also Ref. [7]), a formalism which accounts for both coherent and incoherent processes was formulated, and it was found that the incoherent contribution is essentially larger than the coherent one in the full bremsstrahlung emission. Moreover, the inclusion of incoherent processes in the formalism improves the agreement between the calculated cross section and experimental data [8] for $p + {}^{197}\mathrm{Au}$ at the proton beam energy $E_\mathrm{p} = 190$ MeV. Another useful advance of the incoherent bremsstrahlung is the explanation of a plateau in the middle part of the experimental cross section [8], while the coherent contribution gives only the logarithmic behavior of the calculated cross section that is not enough for a good description of the data [8]. In such a formalism, the full operator of emission of bremsstrahlung photons can be explicitly separated into two groups of terms. One group (coherent bremsstrahlung) includes terms with the momentum defined based on the relative distance between the center of mass of the nucleus target and the scattered proton (for example, for α-nucleus scattering, this is Eq. (B10) in Ref. [7]). The second group (incoherent bremsstrahlung) includes the remaining terms without the momentum from the relative distance between the nucleus target and the scattered proton. But it includes the momenta of relative distances between individual nucleons of the nucleus target and the scattered proton (for α-nucleus scattering, this is Eq. (B11) with addition of Eq. (B12) in Ref. [7]). In other words, the incoherent bremsstrahlung originates from the many-nucleon dynamics, while the coherent bremsstrahlung is related to the two-body (proton-nucleus) dynamics.

So, consideration of nuclear scattering as a many-nucleon quantum mechanical problem allows one to increase significantly the accuracy of the description of bremsstrahlung spectra. Another useful result from those investigations is understanding of important role of magnetic moments of nucleons in nuclei participating in reactions. Attempts to determine accurately relations between parameters of individual nucleons in the studied nuclear process and emission of bremsstrahlung photons give a deeper understanding about nuclear interactions. This motivates us to construct the full cluster formalism for nucleon-nucleus and nucleus-nucleus scattering in the bremsstrahlung problem.

We remind the reader about investigations of bremsstrahlung emission in reactions with light nuclei on the basis of cluster models. Such investigations reveal new information about the wave functions of two colliding nuclei. This process is complementary to the capture reaction or photodisintegration. But, in contrast to these processes, bremsstrahlung is more complicated from a numerical point of view, as calculation of the cross section involves two wave function of states in the continuous energy region. This

*sergei.maydanyuk@wigner.hu
†vsvasilevsky@gmail.com

TABLE I. Nuclei and clusterizations used in investigations of bremsstrahlung in nuclear scattering on the basis of microscopic two-cluster models.

Nucleus	Clusterization	Papers
^{8}Be	$\alpha+\alpha$	[9], [12], [14], [15], [16], [18], [19], [21]
^{7}Be	$\alpha+{}^{3}$He	[10], [13]
^{5}Li	$\alpha+p$	[11], [13], [19], [20]

process has been investigated within microscopic two-cluster models [9–21] (see also Ref. [22]). In Table I we collect all available information about such investigations. The first investigation was performed in Ref. [9], where interaction of two α particles was considered. Theoretical data were obtained for the initial energy of interacting α particles with $E_i \leqslant 10$ MeV. The different geometries of reactions were discussed in detail and the optimal geometry of experiments was recommended. In Ref. [18] the same model was applied to study the bremsstrahlung in α-α collisions with a realistic nucleon-nucleon potential. A wider energy range of two α particles ($E_i \leqslant 50$ MeV) was analyzed. The bremsstrahlung emission in the $\alpha+{}^{3}$He collision was studied in Ref. [10] within the resonating group method. Contributions of the narrow resonance states $7/2^-$ and $5/2^-$ to the bremsstrahlung cross sections are thoroughly studied.

The resonating group method was applied in Ref. [11] to investigate the bremsstrahlung process in the interaction of protons with an α particle. The model correctly reproduced the phase shift of elastic $p+\alpha$ scattering and the parameters of the $3/2^-$ and $1/2^-$ resonance states in ^{5}Li. A good agreement between available experimental data and results of calculations was achieved. The bremsstrahlung cross section was calculated for the energy of the incident proton $0 \leqslant E_p \leqslant 25$ MeV.

There is a significantly larger volume of the experimental bremsstrahlung data obtained with higher precision which has not been analyzed yet by the cluster models. These are data [8] for proton-nucleus scattering (for $p+{}^{197}$Au at proton beam energy $E_{\rm p} = 190$ MeV and inside the photon energy region $E_\gamma = 40$–170 MeV; see also Refs. [23–27]), data [28,29] for α decay of ^{210}Po (see also Refs. [30–34] for nuclei ^{210}Po, ^{214}Po, ^{226}Ra, and ^{244}Cm), and data [35,36] for the spontaneous fission of heavy nuclei ^{252}Cf (see also Refs. [37–42]). There are experimental investigations of the dipole γ-ray emission with incident energy in the ^{32}S + ^{100}Mo and ^{36}S + ^{96}Mo fusion reactions at $E_{\rm lab} = 196$ and 214.2 MeV, respectively, aiming to probe the evolution of fusion with incident energy [43]. γ decays of the excited states in the energy region of the pygmy dipole states in heavy nuclei have been observed [44] (see also Ref. [45]).

Note that the most of the efforts by researchers were on the study of bremsstrahlung in proton-nucleus scattering and fission. But, a strict cluster formalism has not been constructed yet to describe those processes up to the level of a good description of the available experimental data. Some authors have indicated interest in realizing this approach [46]. Note that in microscopic models of α decay [47–54], however, emission of bremsstrahlung photons has not been studied on the basis of those approaches. Emission of bremsstrahlung during the ternary fission of heavy nuclei ^{252}Cf [55] was investigated also. It was found in that paper that the bremsstrahlung spectra are significantly dependent on the different scenarios of dynamics of fission, whch can be studied by means of bremsstrahlung analysis. Hypernuclei in scattering have been studied via analysis of bremsstrahlung emission [7]. However, those investigations were performed without a cluster basis.

Summarizing all the issues above, we see an attractive prospect of constructing a unified formalism and of describing the available experimental information about bremsstrahlung in nuclear reactions. The first step in realization of this program is the aim of this paper, where we focus on the scattering of nuclei with a small number of nucleons in the folding approximation.

The paper is organized in the following way. In Sec. II a new cluster model of emission of bremsstrahlung photons in the scattering of light nuclei is formulated. In Sec. III the folding approximation of the cluster model is described with the main formulas for calculations for s nuclei. In Sec. IV emission of bremsstrahlung photons for scattering is studied on the basis of the model above. Here, we analyze parameters which have significant influence on the accuracy of calculations of the spectra, we calculate the spectra in dependence on the kinetic energy of relative motion between two nuclei in a wide energy region, we estimate the spectra for different nuclei at the same energy of relative motions between nuclei, we analyze the role of the oscillator length of nuclei in calculations of the spectra, we look for sensitivity of the shape of the spectra to the nuclear component of the interaction potential, and we describe the experimental bremsstrahlung data for proton-deuteron scattering on the basis of the model. Conclusions and perspectives are summarized in Sec. V. Useful details of the model are presented in appendices. In these sections we give a formalism and calculations of the matrix elements in the folding approximation (see Appendix A), multiple expansion of the matrix elements of bremsstrahlung (see Appendix B), formalism of polarizations of the emitted photon (see Appendix C), and calculation of angular integrals (see Appendix D).

II. CLUSTER FORMALISM

To study the bremsstrahlung emission in interacting light nuclei, we are going to employ cluster models. First, we need to clarify the term *cluster model*. By the cluster model we mean one of numerous realizations (versions) of the resonating group method (RGM). The resonating group method suggests that the properties of atomic nuclei and various types of nuclear reactions can be described by assuming there are stable formations of nucleons composing clusters. The nucleon-nucleon interaction of nucleons belonging to different clusters creates cluster-cluster interactions. The main differences of various types of the RGM consist of (i) various shapes of wave functions describing the internal structure of the clusters, and (ii) various algorithms for solving the many-particle Schrödinger equation or the equivalent

effective two-body equations of the RGM derived by Wheeler [56,57].

Note that models that treat clusters as structureless particles will be called *potential models*.

Now, let us consider interaction between clusters when antisymmetrization is taken into account or neglected. More precisely, we employ totally antisymmetric functions for a two-cluster configuration $A = A_1 + A_2$,

$$\Psi^{(A)} = \widehat{\mathcal{A}}\{\Phi_1(A_1)\,\Phi_2(A_2)\,\phi\,(\mathbf{r})\}, \tag{1}$$

and also the functions of the so-called *folding model*,

$$\Psi^{(F)} = \Phi_1(A_1)\,\Phi_2(A_2)\,\phi\,(\mathbf{r}), \tag{2}$$

when antisymmetrization of nucleons of different clusters is neglected. To describe relative motion of clusters, one can use the distance $\mathbf{r}$ between clusters,

$$\mathbf{r} = \left[\frac{1}{A_1}\sum_{i\in A_1}\mathbf{r}_i - \frac{1}{A_2}\sum_{j\in A_2}\mathbf{r}_j\right]. \tag{3}$$

It is assumed that the wave functions $\Phi_i(A_i)$, describing internal structure of clusters, are translatoinally invariant and antisymmetric ones. In Eq. (1), the antisymmetrization operator $\widehat{\mathcal{A}}$ permutes nucleons between clusters and thus realizes the Pauli principle correctly. It is well known that the Pauli principle plays an important role especially in the low-energy region of interacting clusters. This approximation we will call the standard version of the resonating group method (RGM). The second approximation which is presented by wave function (2) is called the folding model (FM) or folding approximations.

In what follows, wave functions $\phi(\mathbf{r})$ are to represented in the spherical coordinates

$$\phi(\mathbf{r}) = R_{El}(r)Y_{lm}(\widehat{\mathbf{r}}), \tag{4}$$

where $\widehat{\mathbf{r}} = \mathbf{r}/r$, $|\mathbf{r}| = r$. Wave functions (1) and (2) suggest approximate solutions for the Schrödinger equation,

$$(\widehat{H} - E)\Psi^{(A)} = 0, \tag{5}$$

$$(\widehat{H} - E)\Psi^{(F)} = 0, \tag{6}$$

with a microscopic Hamiltonian $\widehat{H}$ which consists of the kinetic energy operator in the center-of-mass motion and a sum of pairwise nucleon-nucleon potentials.

By multiplying these equations from the left on the product $\Phi_1(A_1)\,\Phi_2(A_2)$ and integrating over internal spatial, spin, and isospin coordinates of nucleons, we obtain an integrodifferential equation for $\phi(\mathbf{q})$ when the Pauli principle is treated correctly, or a differential equation when the folding approximation is used. The later can be written as

$$\left\{-\frac{\hbar^2}{2m_N\mu}\Delta_{\mathbf{r}} + \widehat{V}^{(F)}(\mathbf{r}) - E\right\}\phi(\mathbf{r}) = 0, \tag{7}$$

where μ is the reduced mass,

$$\mu = \frac{A_1A_2}{A_1 + A_2}, \tag{8}$$

and m_N is the mass of a nucleon. It is important to underline that the folding potential $\widehat{V}^{(F)}(\mathbf{r})$ is a key component of a nonlocal intercluster potential appeared in the standard version of the RGM. The folding potential $\widehat{V}^{(F)}(\mathbf{r})$ is totally determined by the shape of the nucleon-nucleon potential and density distributions of nucleons in each cluster.

A. Potential in the folding approximation

In the folding approximation, as pointed out above, the intercluster potential is local and may be easily calculated, especially when simple shell-model functions $\Phi_i(A_i)$ are used to describe the internal state of clusters.

The folding potential is the integral

$$\widehat{V}^{(F)}(\mathbf{r}) = \sum_{i\in A_1}\sum_{j\in A_2}\int dV_1\,dV_2\;|\Phi(A_1)|^2\,\widehat{V}(\mathbf{r}_i - \mathbf{r}_j)\,|\Phi(A_2)|^2, \tag{9}$$

where integration is performed over all coordinates

$$dV_1 = \prod_{i\in A_1} d\mathbf{r}_i, \quad dV_2 = \prod_{i\in A_2} d\mathbf{r}_i. \tag{10}$$

As wave functions $\Phi_1(A_1)$ and $\Phi_2(A_2)$ are translationally invariant, they actually depend on coordinates

$$\mathbf{r}'_i = \mathbf{r}_i - \mathbf{R}_1, \quad \mathbf{R}_1 = \frac{1}{A_1}\sum_{i\in A_1}\mathbf{r}_i, \quad i \in A_1,$$

$$\mathbf{r}'_j = \mathbf{r}_j - \mathbf{R}_2, \quad \mathbf{R}_2 = \frac{1}{A_2}\sum_{j\in A_2}\mathbf{r}_j, \quad j \in A_2, \tag{11}$$

respectively. Thus we have to switch to these coordinates:

$$\widehat{V}^{(F)}(\mathbf{r}) = \sum_{i\in A_1}\sum_{j\in A_2}\int dV'_1\,dV'_2\;|\Phi(A_1)|^2\,\widehat{V}(\mathbf{r}'_i - \mathbf{r}'_j + \mathbf{r}) \times |\Phi(A_2)|^2, \tag{12}$$

where

$$\mathbf{r} = \mathbf{R}_1 - \mathbf{R}_2 = \frac{1}{A_1}\sum_{i\in A_1}\mathbf{r}_i - \frac{1}{A_2}\sum_{j\in A_2}\mathbf{r}_j,$$

$$dV'_1 = \prod_{i\in A_1} d\mathbf{r}'_i, \qquad dV'_2 = \prod_{j\in A_2} d\mathbf{r}'_j \tag{13}$$

and $\Phi(A_\alpha)$ is a many-particle shell model function, describing internal motion of A_α nucleons. As we deal with the two-body potential, we can perform integration over all single-particle coordinates $\mathbf{r}'_i$ ($\mathbf{r}'_j$) but one. As a result integration over all but one coordinates leads us to the density distribution

$$\rho_\alpha(\mathbf{r}) = \int dV'_\alpha\Phi_\alpha(A_\alpha)\sum_i \delta(\mathbf{r} - \mathbf{r}'_i)\Phi_\alpha(A_\alpha). \tag{14}$$

And thus

$$\widehat{V}^{(F)}(\mathbf{r}) = \int d\mathbf{r}_1\,d\mathbf{r}_2\,\rho_1(\mathbf{r}_1)\widehat{V}(\mathbf{r}_1 - \mathbf{r}_2 + \mathbf{r})\,\rho_2(\mathbf{r}_2). \tag{15}$$

For s nuclei, the density distribution equals

$$\rho_\alpha(\mathbf{r}_\alpha) = N_\alpha \exp\left\{-\frac{r^2}{b^2}\frac{A_\alpha}{A_\alpha - 1}\right\}, \tag{16}$$

where b is the oscillator length.

By using Fourier transformation we can reduce (15) to the form

$$\widehat{V}^{(F)}(\mathbf{r}) = \int d\mathbf{k}\, \mathcal{V}(\mathbf{k}) \exp\{i\,\mathbf{k}\,\mathbf{r}\}\, \Phi_1(\mathbf{k})\, \Phi_2(\mathbf{k}). \tag{17}$$

Here, $\mathcal{V}$ denotes the Fourier transform of a nucleon-nucleon interaction,

$$\widehat{V}(\mathbf{r}) = (2\pi)^{-3/2} \int d\mathbf{k}\, \exp\{-i\mathbf{k}\mathbf{r}\}\, \mathcal{V}(\mathbf{k}), \tag{18}$$

and $\Phi_\alpha(\mathbf{k})$ denotes the form factor of a subsystem with A_α nucleons. For the s-shell nuclei, it easy to find that

$$\Phi_\alpha(\mathbf{k}) = \exp\left\{-\frac{k^2 b^2}{4}\,\frac{A_\alpha - 1}{A_\alpha}\right\}. \tag{19}$$

For a nucleon-nucleon interaction, having Gaussian form

$$\widehat{V}(ij) = V_0\, \exp\left\{-\frac{(\mathbf{r}_i - \mathbf{r}_j)^2}{a^2}\right\}, \tag{20}$$

all calculation can be done analytically in closed form and the result reads

$$\widehat{V}^{(F)}(\mathbf{r}) = V_0\, z^{3/2} \exp\left\{-\frac{r^2}{a^2} z\right\}, \tag{21}$$

where

$$z = \left(1 + \frac{b^2}{a^2}[2 - \mu^{-1}]\right)^{-1}. \tag{22}$$

It is worthwhile to notice that when ratio b^2/a^2 is rather small (which takes place for a very wide potential well), then $z \approx 1$ and the folding potential almost coincides with the nucleon-nucleon potential. In other limit case, when $b^2/a^2 \gg 1$ (which may be realized for a potential with small core radius), intensity as well as radius of the potential are significantly redetermined.

B. Case of two-cluster systems

The general formulas obtained above may be adopted to the case of interest, namely, to two-cluster systems. Here we consider two-cluster systems where one of the clusters is an α particle ($A_1 = 4$) and the second cluster consists of A_2 nucleons with $1 \leqslant A_2 \leqslant 4$. In this case we can write

$$V^{(F)}_{NN} = \frac{A_2}{4}(9V_{33} + 3V_{31} + 3V_{13} + V_{11})\left(1 + \frac{b^2}{a^2}\frac{3}{4}\right)^{-3/2} \exp\left\{-\frac{R^2}{a^2}\left(1 + \frac{b^2}{a^2}\frac{3}{4}\right)^{-1}\right\}, \tag{23}$$

$$V^{(F)}_{NN}(\mathbf{r}) = \frac{A_2}{4}(9V_{33} + 3V_{31} + 3V_{13} + V_{11}) z^{3/2} \exp\left\{-\frac{R^2}{a^2} z\right\}, \tag{24}$$

where

$$z = \left(1 + \frac{b^2}{a^2}\left[2 - \mu^{-1}\right]\right)^{-1},$$

$$\mu = \frac{A_1 A_2}{A_1 + A_2},$$

and where V_{33}, V_{31}, V_{13}, V_{11} are intensities of the central nucleon-nucleon interaction (denoted as $V_{2S+1,2T+1}$) with fixed values of the spin S and isospin T of interaction nucleons. Each component of the potential is presented by the sum of two or three Gaussians:

$$V_{2S+1,2T+1}(r) = \sum_{i=1}^{N_G} V^{(i)}_{2S+1,2T+1} \exp\left\{-\frac{r^2}{a_i^2}\right\}. \tag{25}$$

Expressions obtained for NN interaction with Gauss spatial form can be easily transformed to the case of the Coulomb forces. For this we shall use the well-known relation

$$\frac{1}{r} = \frac{2}{\sqrt{\pi}} \int_0^\infty dx\, \exp\{-r^2 x^2\}. \tag{26}$$

Then the Coulomb interaction between clusters with numbers of protons Z_1 and Z_2 is

$$\widehat{V}^{(F)}_C(\mathbf{r}) = \frac{Z_1\, Z_2\, e^2}{b}\,\frac{2}{\sqrt{\pi}} \int d\gamma\, z^{3/2} \exp\left\{-\frac{r^2}{b^2}\gamma^2 z\right\}. \tag{27}$$

By introducing new a variable for integration,

$$a = \frac{\sigma\gamma^2}{1 + \sigma\gamma^2}, \quad \sigma = 2 - \mu^{-1}, \tag{28}$$

we obtain the integral

$$\widehat{V}^{(F)}_C(\mathbf{r}) = \frac{Z_1 Z_2 e^2}{b}\,\frac{2}{\sqrt{\pi}}\,\frac{1}{2\sqrt{\sigma}} \int_0^1 da\, a^{-1/2} \exp\left\{-\frac{r^2}{\sigma\, b^2} a\right\}, \tag{29}$$

which leads to the error function

$$\widehat{V}^{(F)}_C(\mathbf{r}) = \frac{Z_1\, Z_2\, e^2}{R}\, \mathrm{erf}\left(\frac{r^2}{\sigma\, b^2}\right). \tag{30}$$

For large values of $R \gg 1$, we have

$$\widehat{V}^{(F)}_C(\mathbf{r}) \approx \frac{Z_1\, Z_2\, e^2}{r}. \tag{31}$$

C. Operator of emission of bremsstrahlung photons

The translation invariant operator of the interaction of a photon with atomic nuclei is

$$\widehat{H}_e\big(\mathbf{k}_\gamma, \varepsilon_\mu\big) = \frac{1}{2}\frac{e\hbar}{m_N c} \sum_{i=1}^{A} \frac{1}{2}(1 + \widehat{\tau}_{iz})[\widehat{\boldsymbol{\pi}}^*_i \mathbf{A}^*(i) + \mathbf{A}^*(i)\widehat{\boldsymbol{\pi}}^*_i], \tag{32}$$

where

$$\mathbf{A}^*(i) = \varepsilon_\mu \exp\{-i\big(\mathbf{k}_\gamma \boldsymbol{\rho}_i\big)\}, \quad \widehat{\boldsymbol{\pi}}^*_i = i\nabla_{\boldsymbol{\rho}_i},$$

$$\boldsymbol{\rho}_i = \mathbf{r}_i - \mathbf{R}_{\mathrm{c.m.}},$$

$$\mathbf{R}_{\mathrm{c.m.}} = \frac{1}{A}\sum_{i=1}^{A} \mathbf{r}_i, \quad \widehat{\boldsymbol{\pi}}_i = \widehat{\mathbf{p}}_i - \widehat{\mathbf{P}}_{\mathrm{c.m.}}, \quad \widehat{\mathbf{P}}_{\mathrm{c.m.}} = \frac{1}{A}\sum_{i=1}^{A} \widehat{\mathbf{p}}_i, \tag{33}$$

and $\mathbf{k}_\gamma$ is the wave vector of the photon and ε_μ is its circular polarization.

It is worthwhile noticing that operator $\widehat{H}_e(\mathbf{k}_\gamma, \varepsilon_\mu)$ has to be projected onto momentum λ which determine the multipolarity of the emitted photon. The projected operator we denote as $\widehat{H}_e^{(\lambda)}(\mathbf{k}_\gamma, \varepsilon_\mu)$. The projected operator $\widehat{H}_e^{(\lambda)}(\mathbf{k}_\gamma, \varepsilon_\mu)$ will be proportional to spherical functions $Y_{\lambda\mu}(\widehat{\mathbf{r}}_i)$. We do not dwell on projection of the operator $\widehat{H}_e(\mathbf{k}_\gamma, \varepsilon_\mu)$; we will project matrix elements of this operator calculated between Slater determinants. Later we will also consider the operator

$$\widehat{H}_0 = \sum_{i=1}^{A} \frac{1}{2}(1 + \widehat{\tau}_{iz}) \exp\{i(\mathbf{k}_\gamma \mathbf{r}_i)\}, \tag{34}$$

which determines emission or absorption of a photon in the capture reaction or photodisintegration reaction, respectively. This operator can be easily projected on quantum number λ:

$$\widehat{H}_0^{(\lambda)} = \sum_{i=1}^{A} \frac{1}{2}(1 + \widehat{\tau}_{iz}) j_\lambda(k_\gamma r_i) Y_{\lambda\mu}(\widehat{\mathbf{r}}_i). \tag{35}$$

To calculate matrix elements of the operator between Slater determinant wave functions, it is more expedient to use the single-particle operator

$$\widehat{\widehat{H}}_e(\mathbf{k}_\gamma, \varepsilon_\mu) = -\frac{1}{2}\frac{e\hbar}{m_N c} \sum_{i=1}^{A} \frac{1}{2}(1 + \widehat{\tau}_{iz})[\varepsilon_\mu \exp\{-i(\mathbf{k}_\gamma \mathbf{r}_i)\}\widehat{\mathbf{p}}_i^*]. \tag{36}$$

After calculations we obtain

$$\widehat{\widehat{H}}_e(\mathbf{k}_\gamma, \varepsilon_\mu) = -\frac{1}{2}\frac{e\hbar}{m_N c} \sum_{i=1}^{A} \frac{1}{2}(1 + \widehat{\tau}_{iz})[\varepsilon_\mu \exp\{-i(\mathbf{k}_\gamma, \mathbf{r}_i - \mathbf{R}_{\text{c.m.}})\}(\widehat{\mathbf{p}}_i^* - \widehat{\mathbf{P}}_{\text{c.m.}})] \times \exp\{-i(\mathbf{k}_\gamma, \mathbf{R}_{\text{c.m.}})\}$$
$$- \frac{1}{2}\frac{e\hbar}{m_N c} \sum_{i=1}^{A} \frac{1}{2}(1 + \widehat{\tau}_{iz}) \exp\{-i(\mathbf{k}_\gamma, \mathbf{r}_i - \mathbf{R}_{\text{c.m.}})\} \times \exp\{-i(\mathbf{k}_\gamma, \mathbf{R}_{\text{c.m.}})\}(\varepsilon_\mu \widehat{\mathbf{P}}_{\text{c.m.}}). \tag{37}$$

D. Cross section of bremsstrahlung emission

We follow papers [10,11] of Liu, Tang, and Kanada to consider the bremsstrahlung emission in light nuclei. The differential cross section of the bremsstrahlung emission in the coplanar laboratory framework is

$$\frac{d\,\sigma^{(1)}}{d\Omega_1\, d\Omega_2\, d\Omega_\gamma} = \frac{E_\gamma}{(2\pi\hbar)^4}\left(\frac{p_f}{\hbar c}\right)\frac{\sin^2\theta_1 \sin^2\theta_2}{\sin^5(\theta_1 + \theta_2)} \frac{1}{2J+1} \sum_{\mu m_i} |\langle \Psi_{E_f l_f} | \hat{H}_\gamma(\mathbf{k}_\gamma, \varepsilon_\mu) | \Psi_{E_i l_i} \rangle|^2. \tag{38}$$

The new version is

$$\frac{d^3\sigma^{(2)}}{d\Omega_1 d\Omega_2 dE_\gamma} = \frac{p_1^4 v_f}{(2\pi\hbar)^4 \hbar} \frac{\sin^2\theta_1 \sin^2\theta_2}{\sin^5(\theta_1 + \theta_2)} \sum_{\mu} |\langle \Psi_{E_f l_f} | \widehat{H}_e(\mathbf{k}_\gamma, \varepsilon_\mu) | \Psi_{E_i l_i} \rangle|^2, \tag{39}$$

where p_1 is the momentum of the incident nucleus (cluster) with A_1 nucleons.

The kinematic relations for initial (E_i) and final (E_f) energies of a two-cluster system and the photon energy (E_γ) are

$$E_i = E_f + E_\gamma \tag{40}$$

and

$$E_\gamma = E_{1,i}\left[1 - \frac{1}{A_2}\frac{A_1 \sin^2\theta_1 + A_2 \sin^2\theta_2}{\sin^2(\theta_1 + \theta_2)}\right], \tag{41}$$

where $E_{1,i}$ is the energy of the incident cluster A_1. Energies (E_i) and (E_f) are determined in the center-of-mass of coordinate system.

III. MATRIX ELEMENTS IN THE FOLDING APPROXIMATION

Matrix element of bremsstrahlung emission of photons for two s-clusters (i.e., for clusters with $1 \leqslant A_\alpha \leqslant 4$ or for n, p, d, ^{3}H, ^{3}He, ^{4}He) is (see Appendix A for details)

$$\langle \Psi_{E_f l_f} | \hat{H}_\gamma(\mathbf{k}_\gamma, \varepsilon_\mu) | \Psi_{E_i l_i} \rangle = \sqrt{\frac{A_2}{A_1 A}} \langle R_{E_f l_f}(r)\, Y_{l_f m_f}(\widehat{\mathbf{r}}_i)| \exp -i \sqrt{\frac{A_2}{A_1 A}} (\mathbf{k}_\gamma, \mathbf{r})\, (\boldsymbol{\varepsilon}_\mu, \hat{\boldsymbol{\pi}}) | R_{E_i l_i}(r)\, Y_{l_i m_i}(\widehat{\mathbf{r}}_i) \rangle\, F_1$$
$$- \sqrt{\frac{A_1}{A_2 A}} \langle R_{E_f l_f}(r)\, Y_{l_f m_f}(\widehat{\mathbf{r}}_i)| \exp i \sqrt{\frac{A_1}{A_2 A}} (\mathbf{k}_\gamma, \mathbf{r})\, (\boldsymbol{\varepsilon}_\mu, \hat{\boldsymbol{\pi}}) | R_{E_i l_i}(r)\, Y_{l_i m_i}(\widehat{\mathbf{r}}_i) \rangle\, F_2. \tag{42}$$

In the standard approximation of the resonating group method, form factor F_α is ($\alpha = 1, 2$)

$$F_\alpha = \langle \Phi_\alpha(A_\alpha) \big| F_0^{(\alpha)} \big| \Phi_\alpha(A_\alpha) \rangle = Z_\alpha \exp -\frac{1}{4}\frac{A_\alpha - 1}{A_\alpha}(k, b)^2, \tag{43}$$

with b is oscillator length. Thus, to determine cross section of the bremsstrahlung emission, we need to calculate the matrix element ($i = 1, 2$)

$$\mathbf{I}\,(\alpha_i) = \langle R_{E_f l_f}(r)\, Y_{l_f m_f}(\widehat{\mathbf{r}})|\, \exp\{-i\alpha_i(\mathbf{k}_\gamma, \mathbf{r})\}\widehat{\boldsymbol{\pi}}|R_{E_i l_i}(r)\, Y_{l_i m_i}(\widehat{\mathbf{r}})\rangle,$$
$$I_\mu\,(\alpha_i) = \boldsymbol{\varepsilon}_\mu\, \mathbf{I}\,(\alpha_i) = \langle R_{E_f l_f}(r) Y_{l_f m_f}(\widehat{\mathbf{r}})|\, \exp\{-i\alpha_i(\mathbf{k}_\gamma, \mathbf{r})\}(\boldsymbol{\varepsilon}_\mu\widehat{\boldsymbol{\pi}})|R_{E_i l_i}(r)\, Y_{l_i m_i}(\widehat{\mathbf{r}})\rangle \tag{44}$$

for two values of the parameter,

$$\alpha_1 = \sqrt{\frac{A_2}{A_1 A}}, \qquad \alpha_2 = -\sqrt{\frac{A_1}{A_2 A}}. \tag{45}$$

A. Multipole expansion

Applying the multipolar expansion, the integral is [see Appendix B, Eq. (B6)]

$$\mathbf{I}_1(\alpha_i) = \left\langle \phi_f \left| e^{-i\alpha_i \mathbf{k}_\gamma \mathbf{r}} \frac{\partial}{\partial \mathbf{r}} \right| \phi_i \right\rangle_{\mathbf{r}} = \sqrt{\frac{\pi}{2}} \sum_{l_\gamma=1} (-i)^{l_\gamma} \sqrt{2l_\gamma + 1} \sum_{\mu=\pm1} \boldsymbol{\xi}_\mu\, \mu \left[p^M_{l_\gamma \mu} - i\mu\, p^E_{l_\gamma \mu}\right], \tag{46}$$

where (at $l_i = 0$)

$$p^{M0m_f}_{l_\gamma \mu} = -I_M(0, l_f, l_\gamma, 1, \mu) J_1(0, l_f, l_\gamma, \alpha_i),$$
$$p^{E0m_f}_{l_\gamma \mu} = \sqrt{\frac{l_\gamma + 1}{2l_\gamma + 1}} I_E(0, l_f, l_\gamma, 1, l_\gamma - 1, \mu) J_1(0, l_f, l_\gamma - 1, \alpha_i)$$
$$- \sqrt{\frac{l_\gamma}{2l_\gamma + 1}} I_E(0, l_f, l_\gamma, 1, l_\gamma + 1, \mu) J_1(0, l_f, l_\gamma + 1, \alpha_i), \tag{47}$$

and

$$J_1(l_i, l_f, n, \alpha_i) \quad = \quad \int_0^{+\infty} \frac{dR_i(l_i, r)}{dr}\, R^*_f(l_f, r)\, j_n(\alpha_i kr)\, r^2 dr. \tag{48}$$

Here, $\boldsymbol{\varepsilon}^{(\alpha)}$ are unit vectors of *linear* polarization of the photon emitted ($\boldsymbol{\varepsilon}^{(\alpha),*} = \boldsymbol{\varepsilon}^{(\alpha)}$), $\mathbf{k}_\gamma$ is the wave vector of the photon, and $w_\gamma = k_\gamma c = |\mathbf{k}_\gamma| c$. Vectors $\boldsymbol{\varepsilon}^{(\alpha)}$ are perpendicular to $\mathbf{k}_\gamma$ in the Coulomb gauge. We have two independent polarizations $\boldsymbol{\varepsilon}^{(1)}$ and $\boldsymbol{\varepsilon}^{(2)}$ for the photon with impulse $\mathbf{k}_\gamma$ ($\alpha = 1, 2$). $\boldsymbol{\xi}_\mu$ are *vectors of circular polarization* with opposite directions of rotation (see Ref. [58], Eq. (2.39), p. 42; see also Appendix C). Also we have properties

$$[\mathbf{k}_\gamma \times \boldsymbol{\varepsilon}^{(1)}] = k_\gamma\, \boldsymbol{\varepsilon}^{(2)}, \quad [\mathbf{k}_\gamma \times \boldsymbol{\varepsilon}^{(2)}] = -k_\gamma\, \boldsymbol{\varepsilon}^{(1)}, \quad [\mathbf{k}_\gamma \times \boldsymbol{\varepsilon}^{(3)}] = 0, \quad \sum_{\alpha=1,2,3} [\mathbf{k}_\gamma \times \boldsymbol{\varepsilon}^{(\alpha)}] = k_\gamma\, (\boldsymbol{\varepsilon}^{(2)} - \boldsymbol{\varepsilon}^{(1)}). \tag{49}$$

Also we have the property

$$\sum_{\alpha=1,2} \boldsymbol{\varepsilon}^{(\alpha)} \cdot \mathbf{I}_1(\alpha_i) = \sqrt{\frac{\pi}{2}} \sum_{l_\gamma=1} (-i)^{l_\gamma} \sqrt{2l_\gamma + 1} \sum_{\mu=\pm1} \mu\, h_\mu \left(p^M_{l_\gamma, \mu} + p^E_{l_\gamma, -\mu}\right), \tag{50}$$

where [see Eqs. (C5), Appendix C]

$$h_\pm = \mp \frac{1 \pm i}{\sqrt{2}}, \quad h_- + h_+ = -i\sqrt{2}, \quad \sum_{\mu=\pm1} \mu\, h_\mu = -h_- + h_+ = -\sqrt{2}. \tag{51}$$

B. Case of $l_i = 0, l_f = 1, l_\gamma = 1$

In the case of $l_i = 0$, $l_f = 1$, $l_\gamma = 1$ integral (46) is simplified to

$$\mathbf{I}_1(\alpha_i) = -i\sqrt{\frac{3\pi}{2}} \sum_{\mu=\pm1} \boldsymbol{\xi}_\mu\, \mu \left[p^M_{l_\gamma \mu} - i\mu\, p^E_{l_\gamma \mu}\right], \tag{52}$$

where [see Eqs. (47)]

$$p^{M0m_f}_{l_\gamma \mu} = -I_M(0, 1, 1, 1, \mu) J_1(0, 1, 1, \alpha_i),$$
$$p^{E0m_f}_{l_\gamma \mu} = \sqrt{\frac{2}{3}}\, I_E(0, 1, 1, 1, 0, \mu) J_1(0, 1, 0, \alpha_i) - \sqrt{\frac{1}{3}}\, I_E(0, 1, 1, 1, 2, \mu) J_1(0, 1, 2, \alpha_i). \tag{53}$$

Results of calculation of angular integrals are (we omit details of calculations in this paper)

$$I_E\,(0,1,1,1,0,\mu)=\sqrt{\frac{1}{24\pi}},\quad I_M\,(0,1,1,1,\mu)=0,\quad I_E\,(0,1,1,1,2,\mu)=\frac{47}{240}\sqrt{\frac{3}{2\pi}},\tag{54}$$

and matrix elements (53) are simplified to

$$p^{M0m_f}_{l_\gamma\mu}=0,\quad p^{E0m_f}_{l_\gamma\mu}=\frac{1}{6}\sqrt{\frac{1}{\pi}}J_1(0,1,0,\alpha_i)-\frac{47}{240}\sqrt{\frac{1}{2\pi}}J_1(0,1,2,\alpha_i).\tag{55}$$

We substitute these solutions to Eq. (52) and obtain

$$\mathbf{I}_1(\alpha_i)\quad=\quad-\frac{1}{6}\sqrt{\frac{3}{2}}\left(J_1(0,1,0,\alpha_i)-\frac{47}{40}\sqrt{\frac{1}{2}}J_1(0,1,2,\alpha_i)\right)(\boldsymbol{\xi}_{\mu=+1}+\boldsymbol{\xi}_{\mu=-1}).\tag{56}$$

C. Action on vectors of polarization

Now we calculate the summation over vectors of polarization. We use the definition of vectors of polarization [see Eq. (C1)], and find

$$\boldsymbol{\varepsilon}^{(1)}=\frac{1}{\sqrt{2}}(\boldsymbol{\xi}_{-1}-\boldsymbol{\xi}_{+1}),\quad \boldsymbol{\varepsilon}^{(2)}=\frac{i}{\sqrt{2}}(\boldsymbol{\xi}_{-1}+\boldsymbol{\xi}_{+1}).\tag{57}$$

Using (56), we obtain

$$\boldsymbol{\varepsilon}^{(1)}\cdot(\boldsymbol{\xi}_{\mu=+1}+\boldsymbol{\xi}_{\mu=-1})=0,\quad \boldsymbol{\varepsilon}^{(2)}\cdot(\boldsymbol{\xi}_{\mu=+1}+\boldsymbol{\xi}_{\mu=-1})=i\sqrt{2}.\tag{58}$$

On such a basis, from Eq. (56) we find

$$\boldsymbol{\varepsilon}^{(1)}\cdot\mathbf{I}_1(\alpha_i)=0,\quad \boldsymbol{\varepsilon}^{(2)}\cdot\mathbf{I}_1(\alpha_i)=-i\,\frac{\sqrt{3}}{6}\left(J_1(0,1,0,\alpha_i)-\frac{47}{40}\sqrt{\frac{1}{2}}\,J_1(0,1,2,\alpha_i)\right).\tag{59}$$

Using definition (46) for $\mathbf{I_1}\,(\pm\alpha)$, the matrix element (42) is written as

$$\langle\Psi_{E_fl_f}|\hat{H}_\gamma(\mathbf{k}_\gamma,\boldsymbol{\varepsilon}_\mu)|\Psi_{E_il_i}\rangle=-i\hbar\left\{\sqrt{\frac{A_2}{A_1A}}\,\boldsymbol{\varepsilon}_\mu\,\mathbf{I}_1\left(+\sqrt{\frac{A_2}{A_1A}}\right)F_1-\sqrt{\frac{A_1}{A_2A}}\,\boldsymbol{\varepsilon}_\mu\,\mathbf{I}_1\left(-\sqrt{\frac{A_1}{A_2A}}\right)F_2\right\}.\tag{60}$$

IV. ANALYSIS

Cross sections of the bremsstrahlung emission are determined on the basis of integrals defined in Eqs. (48) [see Eq. (39) or (40), and Eqs. (60) and (59)]. These integrals involve the radial wave functions $R_{El}(r)$. These radial wave functions are calculated numerically by solving the Schrödinger equation with the corresponding potential of interaction between two studied clusters (nuclei). Details of normalization, asymptotic behavior of such wave functions, and their numeric calculations are given in Appendix E. In Fig. 1 such cluster-cluster potentials constructed within our formalism above are presented. These potentials include nuclear and Coulomb components and are determined by using the Minnesota nucleon-nucleon potential [59,60] and formulas (24) and (30). Also in this paper we will restrict ourselves to the bremsstrahlung cross sections integrated over angles.

A. Parameters that strongly influence the accuracy of calculations of the spectra

Achieving the needed accuracy of calculation of the spectra turned out to be important in this problem. As it turned out, just direct calculation of the bremsstrahlung spectra at some chosen parameters of calculations did not give satisfactory convergence in calculations for some nuclei. This makes it necessary to understand what determines the accuracy of calculations and what causes errors in the calculation on a computer. Note that it would seem to be possible to increase the number of intervals in the selected region of integration in order to obtain higher convergent calculations of the spectra. In such a way, we have chosen the minimum number of intervals equal to 4 per one oscillation of the radial wave function. However, it turned out that increasing the number of intervals did not allow us to increase the accuracy of determining the cross section. From the formalism one can see that it is more important to analyze the full integrand function of the radial integral, rather than the wave functions themselves.

The integrand function of the bremsstrahlung matrix element for $^3\mathrm{H}+^4\mathrm{He}$ at relative motion energy 15 MeV is shown in Fig. 2. From the figures one can clearly see that the radial region from zero up to 700 fm is the minimum region that includes complete shapes of all harmonics. However, for calculations of the spectra with minimal satisfactory accuracy it is better to take into account at least a few of these complete shapes. This specifies the minimum value of $R_{\max}$. Hence, it is clear that this parameter cannot be small. For calculations in this paper we chose value $R_{\max}=20\,000$ fm and 2 500 000 intervals for the radial region of integration.

B. Spectra in dependence on kinetic energy of relative motion between two nuclei

First, let us analyze how the spectra are changed in dependence on kinetic energy of relative motion between two nuclei. In Fig. 3 we present the bremsstrahlung cross sections for ^{3}H + ^{4}He in such a dependence in the energy range from 7 to 1000 MeV calculated by our approach. From these figures one can see that our approach gives a unified picture of emission of bremsstrahlung photons inside this wide energy region.

C. Cross sections for different nuclei at the same energy of relative motions between nuclei

Cross sections calculated for $p + {}^4$He, ^{2}H + ^{4}He, ^{3}H + ^{4}He, and ^{3}He + ^{4}He at energy 15 MeV are presented in Fig. 4. From this figure one can see that (at the same energy $E_{\rm kin} = 15$ MeV) (1) the most intensive emission of photons is for $p + {}^4$He, (2) emissions of photons for ^{3}H + ^{4}He and ^{3}H + ^{4}He are very similar, and (3) ^{2}H + ^{4}He emits photons with the smallest intensity. One explanation is in the different ratios between form factors (43) for these systems (more precisely, one can calculate factor $f = \sqrt{A_2/(A_1)} \cdot F_1 - \sqrt{A_1/A_2} \cdot F_2$ for such estimations).

D. Role of oscillator length b of nuclei in calculations of the spectra

Let us analyze how the oscillator length influences of the shape of the spectrum. Oscillator length b is included in the matrix element as

$$\langle \Psi_{E_f l_f} | \hat{H}_\gamma(\mathbf{k}_\gamma, \boldsymbol{\varepsilon}_\mu) | \Psi_{E_i l_i} \rangle = -i\hbar \left\{ \sqrt{\frac{A_2}{A_1 A}}\, \boldsymbol{\varepsilon}_\mu\, \mathbf{I}_1\left(+\sqrt{\frac{A_2}{A_1 A}} \right) F_1 - \sqrt{\frac{A_1}{A_2 A}}\, \boldsymbol{\varepsilon}_\mu\, \mathbf{I}_1\left(-\sqrt{\frac{A_1}{A_2 A}} \right) F_2 \right\},$$

$$F_\alpha = Z_\alpha \, \exp -\frac{1}{4}\, \frac{A_\alpha - 1}{A_\alpha}\, (k, b)^2. \tag{61}$$

One can see that, in order to study influence of the oscillator length on the spectra, the exponent in the second formula in Eqs. (61) should be taken into account in calculations. From this formula one can see that inclusion of the oscillator length suppresses the full bremsstrahlung cross section additionally. Here a natural question arises: How strong is such a suppression or can it be practically invisible? A next question is, where is such an influence the most strong? The simplest way to obtain answers comes from numerical estimations of the exponent in dependence on different energies. More precise information is obtained from calculations of the spectra. The bremsstrahlung spectra with influence of the oscillator length for different energies are shown in Fig. 5. Analyzing such spectra, we conclude the following.

(i) Changes of the bremsstrahlung spectra due to change of the oscillator length are practically not visible for energies below 50 MeV.

(ii) The oscillator length begins to play a visible role for higher energies of the emitted photons (i.e., hundreds of MeV). This requires one to use more large energies of scattering of nuclei. Such highest sensitivity in cross sections at higher energies can be explained by the following. Each matrix element of bremsstrahlung emission includes two wave functions of relative motion, i.e., wave functions for states before emission of a photon and after such an emission. The wave function before emission of a photon is defined according to higher energy of relative motion $E_{\rm kin}$, so its wavelength is shorter, which helps one to distinguish more details (more tiny microstructure) in the shape of the potential with barrier. The wave function after emission of a higher energy photon is defined according to smaller energy $E_{\rm kin}$. That allows one to analyze underbarrier tunneling effects and the shape of the barrier. In the matrix element, properties of these two wave functions are combined. Indeed, this is visible Fig. 5, which confirms suchreasoning.

(iii) There is no sense in analyzing spectra at low energies (energies of photons and energies of relative motion between two incident nuclei). Instead, one needs to choose a window in the high energy region for such analysis. There, cross sections are smaller, essentially, which makes experimental measurements and theoretical calculations more difficuly. This aspect creates its own restriction on maximally large energy, higher than which the study of this question will be not realistic (or impossible).

E. Is it possible to see in the spectra the influence of the nuclear component of the interaction potential and where it occurs?

Let us analyze whether it is possible to see in the spectra of photon emission the influence of parameters of the nuclear part of the interaction potential. Calculations of the spectra for ^{3}H + ^{4}He in dependence on the depth of the nuclear component of the potential are shown in Fig. 6. In the first panel (a), the calculations are given at $E_{\rm kin} = 15$ MeV, where one can chose a region in the range of higher photon energies (10–14 MeV), where there is small visible difference between the spectra (this area in the figure is highlighted with a rectangle). One can see a change in the spectra in dependence on the depth of the nuclear part V_0 of the interaction potential. It would seem that this picture should be good indication

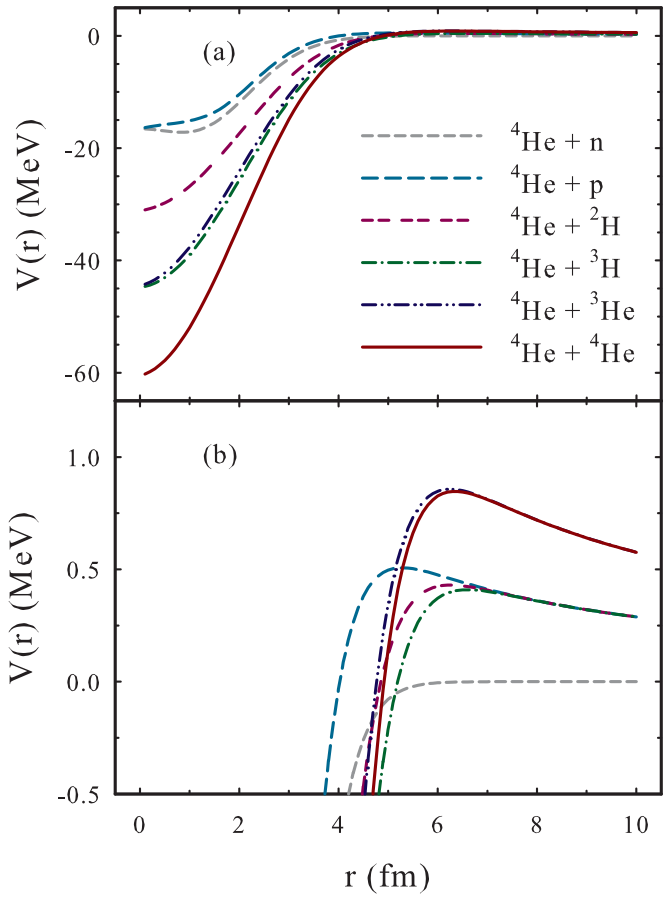

FIG. 1. Potentials for different nuclear systems (see text in Sec. IV for details).

of the place where it is worth looking for the influence of the parameters of the nucleus part of the potential on the bremsstrahlung cross section: *This is a region with higher photon energies (at any energy of relative motion between nuclei)*.

However, let us analyze whether such a dependence will persist with an increase in the energy of the relative motion of the nuclei. The spectra at energy of relative motion of nuclei of 200 MeV are presented in Fig. 6(b). Here one can clearly see another region in the range 25–130 MeV where the difference between the spectra is manifested. Note that this type of relationship has never been found in the study of bremsstrahlung emission in nuclear reactions. Such a dependence is likely to have opposite character than the previous dependence revealed in Fig. 6(a). Apparently, this dependence is more suitable for experimental investigations, because it allows the use of significantly lower photon energies for measurements. This dependence is much more reliable (i.e., it appears in a wider region of photon energies). The spectra have more intense emission, which is easier to measure and gives higher convergence in computer calculations. If, after such a detection of dependence at $E_{\rm kin} = 200$ MeV, one goes back to Fig. 6(a) at $E_{\rm kin} = 15$ MeV, then one can find a suitable difference between spectra of a similar nature for lower photon energies (at 2–6 MeV). This reinforces confidence in the analysis obtained.

F. Analysis of experimental bremsstrahlung data

1. Bremsstrahlung in proton-deuteron scattering

We will analyze bremsstrahlung from proton-deuteron scattering. There are different aspects of using angles in calculations of the bremsstrahlung cross sections. Moreover, in different papers authors sometimes used renormalized experimental data for that reaction. But, one can obtain an understanding about the general tendency of bremsstrahlung cross section from normalized calculations. For this reason reason, we will provide normalized calculations of spectra in this paper. Calculations of bremsstrahlung spectra on the basis of our model in comparison with experimental data of Clayton *et al.* [61] are presented in Fig. 7. From this figure one can see that our approach describes the general trend of these data in Ref. [61] with good enough agreement. One can suppose improved agreement between our calculations and experimental data [61] in the middle part of the spectra if one adds the influence of magnetic moments of nucleons (related to spins of these nucleons) on emission of photons.

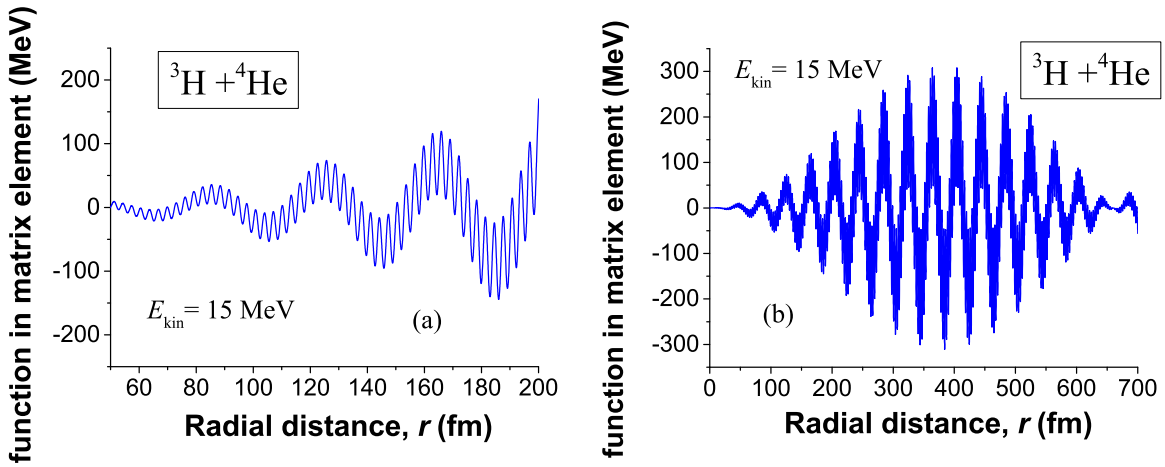

FIG. 2. Shape of the full integrand function of the bremsstrahlung matrix element for ^{3}H + ^{4}He at of relative motion energy 15 MeV in the center-of-mass system. [Parameter of calculations: energy of photons is chosen as 4 MeV for demonstration.]

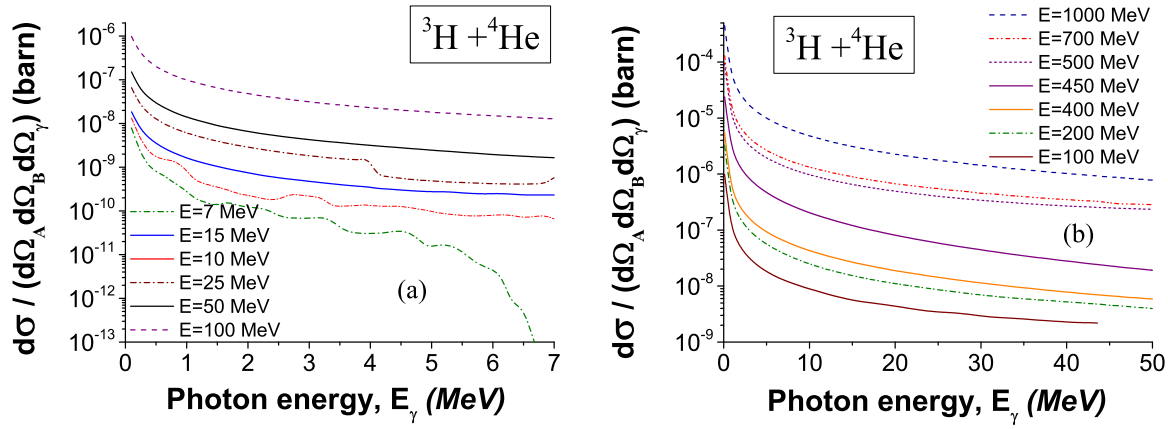

FIG. 3. Cross sections of bremsstrahlung emission for ^{3}H + ^{4}He at different kinetic energies $E_{\rm kin}$ of relative motion. [Parameters of calculations: cross section is defined in Eq. (38), $R_{\rm max} = 20\,000$ and 2 500 000 intervals are chosen in the numerical integration. Time of computer calculation is 53 min for each cross section in panel (a) (50 points for each cross section), and 1 h 12 min for each cross section in panel (b) (70 points for each cross section).] One can see the tendency in each figure that the spectra increase monotonically with increasing energy of relative motion, $E_{\rm kin}$. There is an essential decrease of the cross section with increasing energy of photons for the smallest energy $E_{\rm kin} = 7$ MeV in panel (a), that is explained by tending to the kinematic limit at higher energies of photons. The rate of increase of the spectra with energy $E_{\rm kin}$ is not monotonic, and one can find maxima at some energies.

For comparative analysis we add also the calculation [62] of Herrmann, Speth, and Nakayama, which was used in analysis in Ref. [61]. After renormalization, the general tendency of the spectra are not changed actually (differences are very small). For this reason, we think that our calculation is in better agreement with experimental data [61] than the calculation in [62] (see the red dashed line in the figure).

2. *Bremsstrahlung in the scattering of α-particles on protons*

In this section we will analyze bremsstrahlung emission in the scattering of α particles on protons. Photons of bremsstrahlung were measured over a large range for the reaction of α particles with protons, using the photon spectrometer TAPS at the AGOR facility of the Kernfysisch Verneller Institut [63]. In this experiment a beam of 200 MeV α particles was incident on a liquid hydrogen target. Experimental bremsstrahlung data for this study were presented in papers [63,64] and Ph.D. thesis [65].

From these presented data we choose data in Fig. 3 in Ref. [63] for analysis. Note that inclusive data given in Fig. 1 and exclusive data given in Fig. 3 in that paper are different at $E_\gamma < 20$ MeV (with smaller difference at $E_\gamma > 20$ MeV). We explain our choice by the following. (1) Data in Fig. 3 in Ref. [63] were obtained on the basis of double and triple coincidences. (2) On the basis of these data authors of that paper obtained information about resonances (radiative capture populating the unbound ground and first excited states) of the short-lived nucleus ^{5}Li, extracted the parameters presented in Table I in Ref. [63], and calculated the bremsstrahlung contributions for these resonances shown in Fig. 1 in that paper.

As shown in Ref. [63], for explanation of experimental data one needs to take into account the presence of two unbound states of ^{5}Li for capture in addition to the main bremsstrahlung emission during $p + \alpha$ scattering (it is clearly seen in Figs. 1 and 3 in that paper). In particular, in Fig. 1 in Ref. [63] such states were obtained as two Gaussian peaks. Parameters of these Gaussian peaks were deduced using a fitting procedure (see Table I in that paper). In our paper we do not take into account the incoherent part and magnetic part of bremsstrahlung. So, our approach reproduces the main contribution during scattering, but to take into account two resonant states of ^{5}Li we follow the results of research in [63]. Calculations of bremsstrahlung spectra on the basis of our model in comparison with experimental data of Hoefman *et al.* [63] are presented in Fig. 8.

Our model calculates main bremsstrahlung contribution on a microscopic basis, while in Ref. [63] this contribution was obtained on the basis of phenomenological formula (1) from classical electrodynamics with energy and momentum conservations. The summarized full cross section from our calculations is shown in Fig. 8(b) by a red solid line. One can see that agreement between such our calculated full cross section and experimental data [63] is comparable with the result in Ref. [63]. Also we add the full bremsstrahlung cross section in the low energy region of photons (in contrast to Ref. [63]).[1]

[1]The presence of a visible smooth hump in the calculated cross section at photon energy close to 16 MeV can be explained by restriction of the numerical calculation of Coulomb functions in the close asymptotic region. Note that Coulomb functions at some parameters are calculated on the basis of asymptotic series. These series are not convergent, in principle. But the best calculated values are adequate approximations and they are generally accepted in the physics community for use. However, this results in the origin of small changes in the full bremsstrahlung spectra at some parameters. We suppose that the accuracy of calculation of this part of the cross section can be improved on the basis of the technique developed in Appendix in Ref. [36]. However, this technically solid development is omitted in this paper, and we restrict ourselves to the current accuracy of these functions.

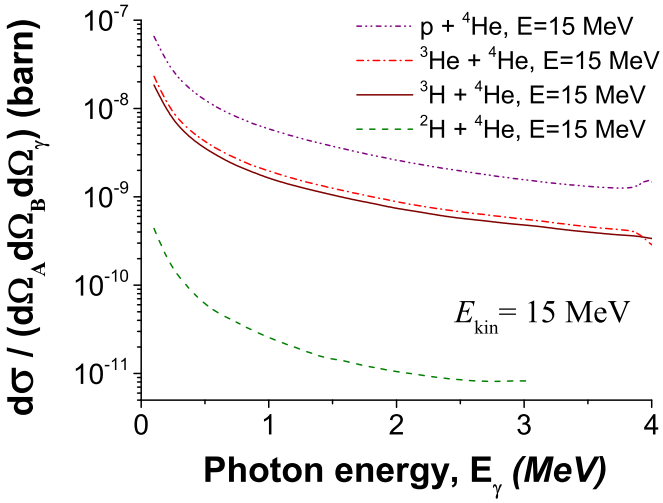

FIG. 4. Cross sections of bremsstrahlung emission for $p + {}^4\mathrm{He}$, ${}^2\mathrm{H} + {}^4\mathrm{He}$, ${}^3\mathrm{H} + {}^4\mathrm{He}$, and ${}^3\mathrm{He} + {}^4\mathrm{He}$ at relative motion kinetic energy $E_{\mathrm{kin}} = 15$ MeV in the center-of-mass frame. [Parameters of calculations: cross sections are defined in Eq. (38), $R_{\max} = 20\,000$ fm, and 2 500 000 intervals are chosen in the numerical integration; time of computer calculation for each cross section is 53 min].

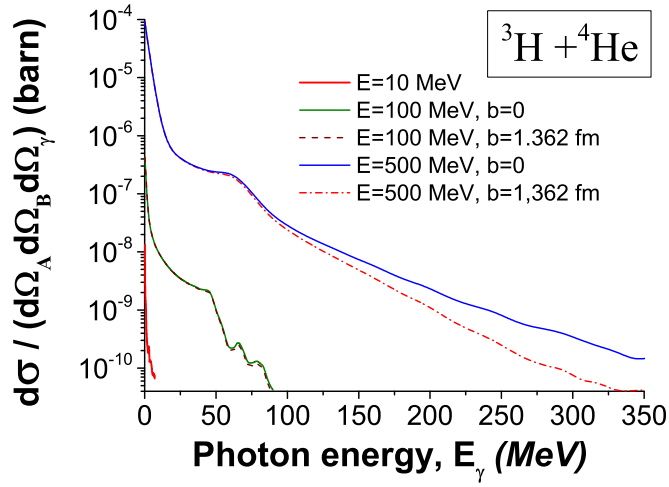

FIG. 5. Cross section of bremsstrahlung emission for ${}^3\mathrm{H} + {}^4\mathrm{He}$ at different oscillator lengths b. [Parameters of calculations: cross section is defined in Eq. (38), $R_{\max} = 10\,000$ fm, and 5 000 000 intervals are chosen in the numerical integration.]

Note that for analysis the authors of [63] also used the potential model of Baye *et al.* [14], the covariant generalization of the Feshbach-Yennie approach based on Refs. [66,67], and a model of direct capture into unbound states based on Ref. [68] (see Fig. 3 in Ref. [63]). However, our microscopic model improves the accuracy of the prediction of the experimental trend at low photon energy with respect to the model used in Ref. [63].

V. CONCLUSIONS AND PERSPECTIVES

In this paper, a new model of the bremsstrahlung emission during light nuclei scattering is constructed with the main focus on the strict cluster formulation of nuclear processes. The analysis is performed within the framework of the folding approximation of the formalism with participation of s nuclei. On the basis of such a model, the emission of bremsstrahlung photons during the scattering of light nuclei is investigated. Conclusions of this study are the following.

(1) Using the example of ${}^3\mathrm{H} + {}^4\mathrm{He}$, we obtain a unified picture of the emission of bremsstrahlung photons in dependence on the different kinetic energies E_{kin} of the relative motion of two nuclei in a wide energy range from 7 to 1000 MeV, calculated by our approach (see Fig. 3). Cross sections increase with the increase of energy of relative motion, E_{kin}. But, the rate of increase of cross sections as a function of energy E_{kin} is nonmonotonic, where one can find maxima at some energies.

(2) We estimate a comparable picture of the bremsstrahlung emission for $p + {}^4\mathrm{He}$, ${}^2\mathrm{H} + {}^4\mathrm{He}$, ${}^3\mathrm{H} + {}^4\mathrm{He}$, and ${}^3\mathrm{He} + {}^4\mathrm{He}$ with the same kinetic energy of relative motion, $E_{\mathrm{kin}} = 15$ MeV (see Fig. 4). The general behavior of the spectra is similar for all systems. We find that (1) the most intensive emission of photons is for $p + {}^4\mathrm{He}$, (2) emissions of photons for ${}^3\mathrm{H} + {}^4\mathrm{He}$ and ${}^3\mathrm{He} + {}^4\mathrm{He}$ are very similar, and (3) ${}^2\mathrm{H} + {}^4\mathrm{He}$ emits photons with the smallest intensity.

(3) The influence of the internal structure of interacting clusters on the cross section of the bremsstrahlung emission is analyzed [see Eqs. (61) and Fig. 5]. Within the present model, the internal structure is contributed through the elastic form factors. We conclude the following.
   (1) The inclusion of cluster form factors further suppresses the full bremsstrahlung cross section.
   (2) Changes in the bremsstrahlung spectra due to change of the internal structure are practically invisible at energies below 50 MeV.
   (3) Cluster form factors begin to play a prominent role for higher energies of the emitted photons (i.e., hundreds of MeV). This requires the use of larger energies of the incident nuclei.
   (4) There is no sense in analyzing the bremsstrahlung cross sections at low energies of the emitted photons as a contribution from the internal structure is negligibly small. Instead, one needs to choose a window in the high-energy region for this analysis. On this point, the cross sections are significantly smaller, which makes experimental measurements and theoretical calculations more difficult. This aspect gives a restriction of the largest possible energy beyond which the study of this question will not seem realistic.

(4) The dependence of the bremsstrahlung spectra on the parameters of the nuclear part of the cluster-cluster potential has been revealed. Using the example of ${}^3\mathrm{H} + {}^4\mathrm{He}$, for better observation of such a dependence, we find two regions in the spectra: the middle-energy

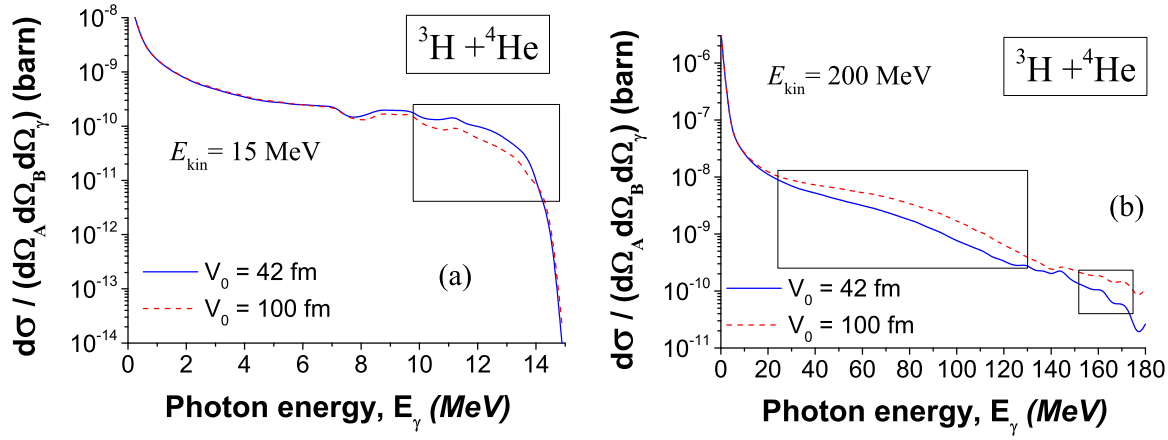

FIG. 6. Cross sections of bremsstrahlung emission for $^3\mathrm{H} + {}^4\mathrm{He}$ in dependence on depth of nuclear potential V_0 at relative motion energyies 15 MeV (a) and 200 MeV (b) in the center-of-mass frame [Parameters of calculations: cross section is defined in Eq. (38), $R_{max} = 2000$ fm, and 2 500 000 intervals are chosen in the numerical integration].

region and the high-energy region (see Fig. 6). In the middle-energy region, the calculations of the spectra are more stable, and intensity of emission is higher which is convenient for possible measurements. In the high-energy region, the dependence is more sensitive to variations of nuclear parameters. But the intensity of the emission is smaller which is problematic for possible measurements and computer calculations.

(5) The bremsstrahlung cross section calculated on the basis of our model for proton-deuteron scattering at $E_p = 145$ MeV is in good agreement with experimental data [61] (see Fig. 7).

(6) The bremsstrahlung emission for the scattering of α particles on protons at the beam energy of α particles $E_\alpha = 200$ MeV was analyzed. The bremsstrahlung cross section obtained by summation of main contributions in the $p + \alpha$ scattering (calculated on the basis of our microscopic model) and two additional contributions from captures at unbound ground and first excited states of ^{5}Li is in good agreement with the general trend of experimental data [63] (see Fig. 8).

As a future prospect, we plan to evaluate the contribution from the inclusion of nucleon magnetic moments in the model. We believe that this should provide an additional new incoherent bremsstrahlung contribution. According to a previous study of bremsstrahlung in the scattering of protons from heavy nuclei [6], this incoherent emission is important and not small. However, its role can be significantly smaller for light nuclei, according to our preliminary estimates. We also estimate that this term can improve agreement between the calculated full cross section and corresponding experimental data.

ACKNOWLEDGMENTS

M.S.P. thanks the Wigner Research Centre for Physics in Budapest for warm hospitality. The authors are highly appreciated to Prof. Gyorgy Wolf for many fruitful discussions concerning to different aspects of nuclear collisions at high energies. This work was supported in part by the Program of Fundamental Research of the Physics and Astronomy Department of the National Academy of Sciences of Ukraine (Project No. 0117U000239). S.P.M. acknowledges the support of OTKA Grant No. K138277.

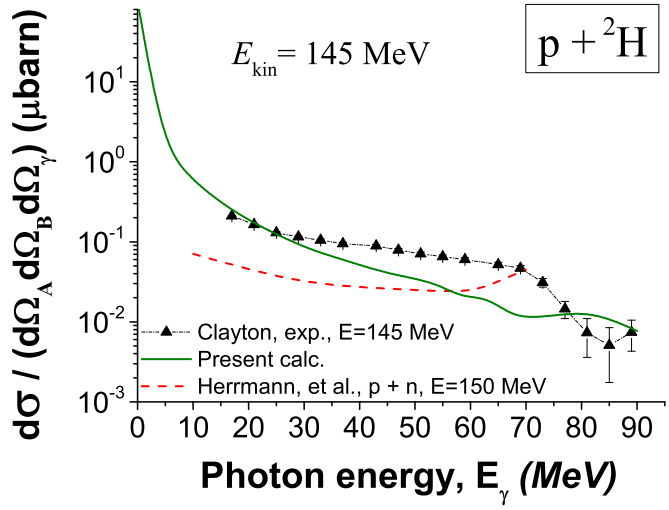

FIG. 7. Normalized cross sections of bremsstrahlung emission for $p + {}^2\mathrm{H}$ at energy of proton beam of 145 MeV in comparison with experimental data [61]. [Parameters of calculations: cross section is defined in Eq. (38), $R_{max} = 20\,000$ fm, and 2 500 000 intervals are used in the numerical integration; kinetic energy E_{kin} of the relative motion of proton and deuteron is used in calculations of bremsstrahlung matrix elements, which is $E_{kin} = (2/3) \times E_p = 98$ MeV.] The bremsstrahlung calculation of Herrmann, Speth, and Nakayama for $p + n$ at 150 MeV [62] is added for comparative analysis (see the red dashed line in the figure).

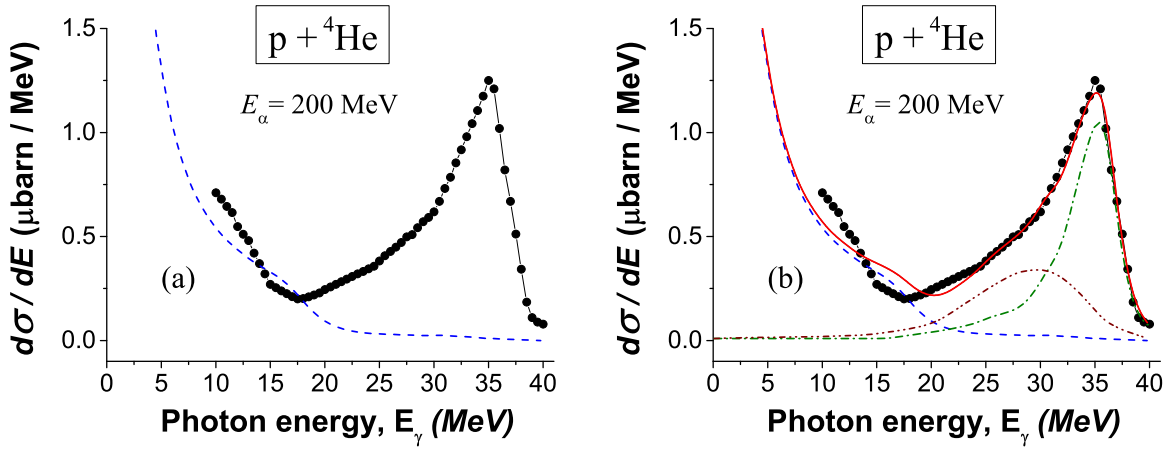

FIG. 8. Calculated cross sections of bremsstrahlung emission for $p + {}^4\mathrm{He}$ at beam energy of the α particles of 200 MeV in comparison with experimental data [63]. [Parameters of calculations: cross section is defined in Eq. (39), $R_{\max} = 20\,000$ fm, and 2 500 000 intervals are used in the numerical integration.] (a) Main bremsstrahlung contribution of photons emitted in the $p + \alpha$ scattering calculated by our model (see blue dashed line) in comparison with experimental data. (b) Full bremsstrahlung cross section (see red solid line) obtained as summation of the main contribution in the $p + \alpha$ scattering (see blue dashed line) and two additional contributions from capture at unbound ground and first excited states of ${}^5\mathrm{Li}$ (see green dash-dotted line and brown dash–double-dotted line) in comparison with experimental data.

APPENDIX A: MATRIX ELEMENT IN THE FOLDING APPROXIMATION

Let us consider the operator

$$\widehat{H}_e(\mathbf{k}_\gamma, \boldsymbol{\varepsilon}_\mu) = \frac{e\hbar}{m_N c} \sum_{i=1}^{A} \frac{1}{2}(1 + \widehat{\tau}_{iz})\mathbf{A}^*(i)\widehat{\boldsymbol{\pi}}_i^* \tag{A1}$$

for a two-cluster system with the partition $A = A_1 + A_2$. In this case the operator $\widehat{H}_e(\mathbf{k}_\gamma, \boldsymbol{\varepsilon}_\mu)$ can be presented as

$$\begin{aligned}\widehat{H}_e(\mathbf{k}_\gamma, \boldsymbol{\varepsilon}_\mu) &= \widehat{H}_e^{(1)}(\mathbf{k}_\gamma, \boldsymbol{\varepsilon}_\mu) + \widehat{H}_e^{(2)}(\mathbf{k}_\gamma, \boldsymbol{\varepsilon}_\mu) \\ &= \frac{e\hbar}{m_N c} \sum_{i\in A_1} \frac{1}{2}(1 + \widehat{\tau}_{iz})\mathbf{A}^*(i)\widehat{\boldsymbol{\pi}}_i^* + \frac{e\hbar}{m_N c} \sum_{j\in A_2} \frac{1}{2}(1 + \widehat{\tau}_{jz})\mathbf{A}^*(j)\widehat{\boldsymbol{\pi}}_j^*.\end{aligned} \tag{A2}$$

It is necessary to recall that

$$\begin{aligned}\mathbf{A}^*(i)\widehat{\boldsymbol{\pi}}_i^* &= \exp\{-i(\mathbf{k}_\gamma \boldsymbol{\rho}_i)\}(\boldsymbol{\varepsilon}_\mu \widehat{\boldsymbol{\pi}}_i^*) \\ &= \exp\{-i(\mathbf{k}_\gamma, \mathbf{r}_i - \mathbf{R}_{\mathrm{c.m.}})\}(\boldsymbol{\varepsilon}_\mu[\widehat{\mathbf{p}}_i^* - \widehat{\mathbf{P}}_{\mathrm{c.m.}}^*]).\end{aligned} \tag{A3}$$

The first operator $\widehat{H}_e^{(1)}(\mathbf{k}_\gamma, \boldsymbol{\varepsilon}_\mu)$ we represent in the following form:

$$\begin{aligned}\widehat{H}_e^{(1)}(\mathbf{k}_\gamma, \boldsymbol{\varepsilon}_\mu) \quad &= \quad \frac{e\hbar}{m_N c} \exp\{-i(\mathbf{k}_\gamma, \mathbf{R}_1 - \mathbf{R}_{\mathrm{c.m.}})\} \sum_{i\in A_1} \frac{1}{2}(1 + \widehat{\tau}_{iz}) \exp\{-i(\mathbf{k}_\gamma, \mathbf{r}_i - \mathbf{R}_1)\}(\boldsymbol{\varepsilon}_\mu[\widehat{\mathbf{p}}_i^* - \widehat{\mathbf{P}}_1^*]) \\ &+ \quad \frac{e\hbar}{m_N c} \exp\{-i(\mathbf{k}_\gamma, \mathbf{R}_1 - \mathbf{R}_{\mathrm{c.m.}})\}(\boldsymbol{\varepsilon}_\mu[\widehat{\mathbf{P}}_1^* - \widehat{\mathbf{P}}_{\mathrm{c.m.}}^*]) \sum_{i\in A_1} \frac{1}{2}(1 + \widehat{\tau}_{iz}) \exp\{-i(\mathbf{k}_\gamma, \mathbf{r}_i - \mathbf{R}_1)\},\end{aligned} \tag{A4}$$

where $\mathbf{R}_1$ and $\widehat{\mathbf{P}}_1^*$ are the coordinate and momentum of center-of-mass motion of the first cluster:

$$\mathbf{R}_1 = \frac{1}{A_1} \sum_{i\in A_1} \mathbf{r}_i, \quad \widehat{\mathbf{P}}_1 = \frac{1}{A_1} \sum_{i\in A_1} \widehat{\mathbf{p}}_i. \tag{A5}$$

In similar way we can present the second operator:

$$\begin{aligned}\widehat{H}_e^{(2)}(\mathbf{k}_\gamma, \boldsymbol{\varepsilon}_\mu) &= \frac{e\hbar}{m_N c} \exp\{-i(\mathbf{k}_\gamma, \mathbf{R}_2 - \mathbf{R}_{\mathrm{c.m.}})\} \sum_{j\in A_2} \frac{1}{2}(1 + \widehat{\tau}_{jz}) \exp\{-i(\mathbf{k}_\gamma, \mathbf{r}_j - \mathbf{R}_2)\}(\boldsymbol{\varepsilon}_\mu[\widehat{\mathbf{p}}_j^* - \widehat{\mathbf{P}}_2^*]) \\ &+ \frac{e\hbar}{m_N c} \exp\{-i(\mathbf{k}_\gamma, \mathbf{R}_2 - \mathbf{R}_{\mathrm{c.m.}})\}(\boldsymbol{\varepsilon}_\mu[\widehat{\mathbf{P}}_2^* - \widehat{\mathbf{P}}_{\mathrm{c.m.}}]) \sum_{j\in A_2} \frac{1}{2}(1 + \widehat{\tau}_{jz}) \exp\{-i(\mathbf{k}_\gamma, \mathbf{r}_j - \mathbf{R}_2)\},\end{aligned} \tag{A6}$$

where

$$\mathbf{R}_2 = \frac{1}{A_2}\sum_{j\in A_2}\mathbf{r}_j, \quad \widehat{\mathbf{P}}_2 = \frac{1}{A_2}\sum_{j\in A_2}\widehat{\mathbf{p}}_j. \tag{A7}$$

Consider in detail the differences

$$\mathbf{R}_1 - \mathbf{R}_{\text{c.m.}}, \quad \mathbf{R}_2 - \mathbf{R}_{\text{c.m.}}. \tag{A8}$$

Taking into account their definitions, we obtain

$$\begin{aligned}
\mathbf{R}_1 - \mathbf{R}_{\text{c.m.}} &= \frac{1}{A_1}\sum_{i\in A_1}\mathbf{r}_i - \frac{1}{A}\sum_{i=1}^{A}\mathbf{r}_i = \sqrt{\frac{A_2}{A_1A}}\sqrt{\frac{A_1A_2}{A}}\left[\frac{1}{A_1}\sum_{i\in A_1}\mathbf{r}_i - \frac{1}{A_2}\sum_{j\in A_2}\mathbf{r}_j\right], \\
\mathbf{R}_2 - \mathbf{R}_{\text{c.m.}} &= \frac{1}{A_2}\sum_{j\in A_2}\mathbf{r}_j - \frac{1}{A}\sum_{i=1}^{A}\mathbf{r}_i = -\sqrt{\frac{A_1}{AA_2}}\sqrt{\frac{A_1A_2}{A}}\left[\frac{1}{A_1}\sum_{i\in A_1}\mathbf{r}_i - \frac{1}{A_2}\sum_{j\in A_2}\mathbf{r}_j\right].
\end{aligned} \tag{A9}$$

Thus

$$\mathbf{R}_1 - \mathbf{R}_{\text{c.m.}} = \sqrt{\frac{A_2}{A_1A}}\mathbf{q}, \quad \mathbf{R}_2 - \mathbf{R}_{\text{c.m.}} = -\sqrt{\frac{A_1}{A_2A}}\mathbf{q}, \tag{A10}$$

where

$$\mathbf{q} = \sqrt{\frac{A_1A_2}{A}}\left[\frac{1}{A_1}\sum_{i\in A_1}\mathbf{r}_i - \frac{1}{A_2}\sum_{j\in A_2}\mathbf{r}_j\right] \tag{A11}$$

is the Jacobi vector determining distance between clusters. Similarly, we can transform momenta

$$\widehat{\mathbf{P}}_1 - \widehat{\mathbf{P}}_{\text{c.m.}} = \sqrt{\frac{A_2}{A_1A}}\widehat{\boldsymbol{\pi}}, \quad \widehat{\mathbf{P}}_2 - \widehat{\mathbf{P}}_{\text{c.m.}} = -\sqrt{\frac{A_1}{A_2A}}\widehat{\boldsymbol{\pi}}, \tag{A12}$$

where

$$\widehat{\boldsymbol{\pi}} = \sqrt{\frac{A_1A_2}{A}}\left[\frac{1}{A_1}\sum_{i\in A_1}\widehat{\mathbf{p}}_i - \frac{1}{A_2}\sum_{j\in A_2}\widehat{\mathbf{p}}_j\right]. \tag{A13}$$

Concluding, we can write down

$$\begin{aligned}
\widehat{H}_e\big(\mathbf{k}_\gamma, \boldsymbol{\varepsilon}_\mu\big) &= \exp\left\{-i\sqrt{\frac{A_2}{A_1A}}(\mathbf{k}_\gamma, \mathbf{q})\right\}\cdot F_1^{(1)} + \frac{e\hbar}{m_Nc}\sqrt{\frac{A_2}{A_1A}}\exp\left\{-i\sqrt{\frac{A_2}{A_1A}}(\mathbf{k}_\gamma, \mathbf{q})\right\}\widehat{\boldsymbol{\pi}}\cdot F_0^{(1)} \\
&+ \exp\left\{i\sqrt{\frac{A_1}{A_2A}}\big(\mathbf{k}_\gamma, \mathbf{q}\big)\right\}\cdot F_1^{(2)} - \frac{e\hbar}{m_Nc}\sqrt{\frac{A_1}{A_2A}}\exp\left\{i\sqrt{\frac{A_1}{A_2A}}(\mathbf{k}_\gamma, \mathbf{q})\right\}\widehat{\boldsymbol{\pi}}\cdot F_0^{(2)},
\end{aligned} \tag{A14}$$

where

$$\begin{aligned}
F_0^{(\alpha)} &= \sum_{i\in A_\alpha}\frac{1}{2}(1+\widehat{\tau}_{iz})\exp\{-i(\mathbf{k}_\gamma, \mathbf{r}_i - \mathbf{R}_\alpha)\}, \\
F_1^{(\alpha)} &= \frac{e\hbar}{m_Nc}\sum_{i\in A_\alpha}\frac{1}{2}(1+\widehat{\tau}_{iz})\exp\{-i(\mathbf{k}_\gamma, \mathbf{r}_i - \mathbf{R}_\alpha)\}(\boldsymbol{\varepsilon}_\mu[\widehat{\mathbf{p}}_i^* - \widehat{\mathbf{P}}_\alpha^*])
\end{aligned} \tag{A15}$$

with $\alpha = 1, 2$.

If we consider a two-cluster system in the folding approximation, then a wave function of the system is

$$\Psi_{El} = \Phi_1(A_1)\Phi_2(A_2)R_{El}(q)Y_{lm}(\widehat{\mathbf{q}}), \tag{A16}$$

where functions $\Phi_1(A_1)$ and $\Phi_2(A_2)$ describe internal motion of nucleons of the first and second clusters, respectively, and $\widehat{\mathbf{q}}$ is a unit vector ($\widehat{\mathbf{q}} = \mathbf{q}/q$). The matrix element of the operator (A14) between functions $\Psi_{E_f l_f}$ and $\Psi_{E_i l_i}$ is then

$$\begin{aligned}\langle\Psi_{E_f l_f}|\widehat{H}_e^{(1)}(\mathbf{k}_\gamma,\boldsymbol{\varepsilon}_\mu)|\Psi_{E_i l_i}\rangle &= \left\langle R_{E_f l_f}(q)Y_{l_f m_f}(\widehat{\mathbf{q}})\middle|\exp\left\{-i\sqrt{\frac{A_2}{A_1 A}}(\mathbf{k}_\gamma,\mathbf{q})\right\}\middle|R_{E_i l_i}(q)Y_{l_i m_i}(\widehat{\mathbf{q}})\right\rangle\langle\Phi_1(A_1)|F_1^{(1)}|\Phi_1(A_1)\rangle\\ &+\sqrt{\frac{A_2}{A_1 A}}\left\langle R_{E_f l_f}(q)Y_{l_f m_f}(\widehat{\mathbf{q}})\middle|\exp\left\{-i\sqrt{\frac{A_2}{A_1 A}}(\mathbf{k}_\gamma,\mathbf{q})\right\}(\boldsymbol{\varepsilon}_\mu\widehat{\boldsymbol{\pi}})\middle|R_{E_i l_i}(q)Y_{l_i m_i}(\widehat{\mathbf{q}})\right\rangle\langle\Phi_1(A_1)|F_0^{(1)}|\Phi_1(A_1)\rangle\\ &+\left\langle R_{E_f l_f}(q)Y_{l_f m_f}(\widehat{\mathbf{q}})\middle|\exp\left\{i\sqrt{\frac{A_1}{A_2 A}}(\mathbf{k}_\gamma,\mathbf{q})\right\}\middle|R_{E_i l_i}(q)Y_{l_i m_i}(\widehat{\mathbf{q}})\right\rangle\langle\Phi_2(A_2)|F_1^{(2)}|\Phi_2(A_2)\rangle\\ &-\sqrt{\frac{A_1}{A_2 A}}\left\langle R_{E_f l_f}(q)Y_{l_f m_f}(\widehat{\mathbf{q}})\middle|\exp\left\{i\sqrt{\frac{A_1}{A_2 A}}(\mathbf{k}_\gamma,\mathbf{q})\right\}(\boldsymbol{\varepsilon}_\mu\widehat{\boldsymbol{\pi}})\middle|R_{E_i l_i}(q)Y_{l_i m_i}(\widehat{\mathbf{q}})\right\rangle\langle\Phi_2(A_2)|F_0^{(2)}|\Phi_2(A_2)\rangle.\end{aligned} \tag{A17}$$

For two s clusters (i.e., for clusters with $1 \leqslant A_\alpha \leqslant 4$ or for n, p, d, t, ^{3}He, and ^{4}He)

$$\langle\Phi_1(A_1)|F_1^{(1)}|\Phi_1(A_1)\rangle = \langle\Phi_2(A_2)|F_1^{(2)}|\Phi_2(A_2)\rangle = 0, \tag{A18}$$

consequently

$$\begin{aligned}\langle\Psi_{E_f l_f}|\widehat{H}_e^{(1)}(\mathbf{k}_\gamma,\boldsymbol{\varepsilon}_\mu)|\Psi_{E_i l_i}\rangle &= \sqrt{\frac{A_2}{A_1 A}}\left\langle R_{E_f l_f}(q)Y_{l_f m_f}(\widehat{\mathbf{q}})\middle|\exp\left\{-i\sqrt{\frac{A_2}{A_1 A}}(\mathbf{k}_\gamma,\mathbf{q})\right\}(\boldsymbol{\varepsilon}_\mu\widehat{\boldsymbol{\pi}})\middle|R_{E_i l_i}(q)Y_{l_i m_i}(\widehat{\mathbf{q}})\right\rangle\langle\Phi_1(A_1)|F_0^{(1)}|\Phi_1(A_1)\rangle\\ &-\sqrt{\frac{A_1}{A_2 A}}\left\langle R_{E_f l_f}(q)Y_{l_f m_f}(\widehat{\mathbf{q}})\middle|\exp\left\{i\sqrt{\frac{A_1}{A_2 A}}(\mathbf{k}_\gamma,\mathbf{q})\right\}(\boldsymbol{\varepsilon}_\mu\widehat{\boldsymbol{\pi}})\middle|R_{E_i l_i}(q)Y_{l_i m_i}(\widehat{\mathbf{q}})\right\rangle\langle\Phi_2(A_2)|F_0^{(2)}|\Phi_2(A_2)\rangle.\end{aligned} \tag{A19}$$

In the standard approximation of the resonating group method (or cluster model), the form factor is

$$\langle\Phi_\alpha(A_\alpha)|F_0^{(1)}|\Phi_\alpha(A_\alpha)\rangle = Z_\alpha\exp\left\{-\frac{1}{4}\frac{A_\alpha-1}{A_\alpha}(k_\gamma b)^2\right\}, \tag{A20}$$

where b is the oscillator length. Thus, to determine the cross section of the bremsstrahlung emission, we need to calculate matrix element

$$I_\mu(\alpha) = \langle R_{E_f l_f}(q)\,Y_{l_f m_f}(\widehat{\mathbf{q}})|\exp\{-i\alpha(\mathbf{k}_\gamma,\mathbf{q})\}(\boldsymbol{\varepsilon}_\mu\widehat{\boldsymbol{\pi}})|R_{E_i l_i}(q)Y_{l_i m_i}(\widehat{\mathbf{q}})\rangle \tag{A21}$$

for two values of the parameter,

$$\alpha_1 = \sqrt{\frac{A_2}{A_1 A}}, \quad \alpha_2 = -\sqrt{\frac{A_1}{A_2 A}}. \tag{A22}$$

APPENDIX B: MULTIPOLE EXPANSION OF MATRIX ELEMENTS

1. Matrix elements integrated over space coordinates

We shall calculate the following matrix elements [see Ref. [5], Eqs. (24)–(41)]:

$$\langle\phi_f|\,e^{-i\alpha_i\mathbf{k}_\gamma\mathbf{r}}\,|\,\phi_i\rangle_{\mathbf{r}} = \int\phi_f^*(\mathbf{r})\,e^{-i\alpha_i\mathbf{k}_\gamma\mathbf{r}}\,\phi_i(\mathbf{r})\,\mathbf{dr}, \qquad \left\langle\phi_f\middle|\,e^{-i\alpha_i\mathbf{k}_\gamma\mathbf{r}}\frac{\partial}{\partial\mathbf{r}}\middle|\,\phi_i\right\rangle_{\mathbf{r}} = \int\phi_f^*(\mathbf{r})\,e^{-i\alpha_i\mathbf{k}_\gamma\mathbf{r}}\frac{\partial}{\partial\mathbf{r}}\,\phi_i(\mathbf{r})\,\mathbf{dr}. \tag{B1}$$

a. Expansion of the vector potential **A** *by multipoles*

Let us expand the vectorial potential **A** of an electromagnetic field by multipoles. According to Ref. [58] [see Eqs. (2.106), p. 58], in the spherical symmetric approximation we have

$$\boldsymbol{\xi}_\mu\,e^{i\alpha_i\mathbf{k}_\gamma\mathbf{r}} = \mu\sqrt{2\pi}\sum_{l_\gamma=1}(2l_\gamma+1)^{1/2}\,i^{l_\gamma}\,[\mathbf{A}_{l_\gamma\mu}(\mathbf{r},M) + i\mu\,\mathbf{A}_{l_\gamma\mu}(\mathbf{r},E)], \tag{B2}$$

where (see [58], Eq. (2.73) on p. 49 and Eq. (2.80) on p. 51)

$$\mathbf{A}_{l_\gamma\mu}(\mathbf{r},M)=j_{l_\gamma}(\alpha_i k_\gamma r)\,\mathbf{T}_{l_\gamma l_\gamma,\mu}(\widehat{\mathbf{r}}),$$
$$\mathbf{A}_{l_\gamma\mu}(\mathbf{r},E)=\sqrt{\frac{l_\gamma+1}{2l_\gamma+1}}\,j_{l_\gamma-1}(\alpha_i k_\gamma r)\,\mathbf{T}_{l_\gamma l_\gamma-1,\mu}(\widehat{\mathbf{r}})\;-\sqrt{\frac{l_\gamma}{2l_\gamma+1}}\,j_{l_\gamma+1}(\alpha_i k_\gamma r)\,\mathbf{T}_{l_\gamma l_\gamma+1,\mu}(\widehat{\mathbf{r}}). \tag{B3}$$

Here, $\mathbf{A}_{l_\gamma\mu}(\mathbf{r},M)$ and $\mathbf{A}_{l_\gamma\mu}(\mathbf{r},E)$ are *magnetic* and *electric multipoles*, $j_{l_\gamma}(\alpha_i k_\gamma r)$ is the *spherical Bessel function of order* l_γ, $\mathbf{T}_{l_\gamma l'_\gamma,\mu}(\widehat{\mathbf{r}})$ are *vector spherical harmonics*, and $\boldsymbol{\xi}_\mu$ are *vectors of circular polarization* of the emitted photon. Equation (B2) is the solution of the wave equation of an electromagnetic field in the form of plane wave, and is presented as the summation of the electrical and magnetic multipoles (for example, see pp. 83–92 in [69]). Therefore, separate multipolar terms in Eq. (B2) are solutions of this wave equation for chosen numbers j_γ and l_γ (j_γ is a quantum number characterizing the eigenvalue of the full momentum operator, while $l_\gamma=j_\gamma-1,\,j_\gamma,\,j_\gamma+1$ is connected with the orbital momentum operator, but it defines eigenvalues of photon parity and so it is a quantum number also).

We orient the frame so that axis z be directed along the vector $\mathbf{k}_\gamma$ (see [58], Eq. (2.105) on p. 57). According to [58] (see p. 45), the functions $\mathbf{T}_{l_\gamma l'_\gamma,\mu}(\widehat{\mathbf{r}})$ have the following form ($\boldsymbol{\xi}_0=0$):

$$\mathbf{T}_{j_\gamma l_\gamma,m}(\widehat{\mathbf{r}})=\sum_{\mu=\pm1}(l_\gamma,1,j_\gamma\,|\,m-\mu,\mu,m)\,Y_{l_\gamma,m-\mu}(\widehat{\mathbf{r}})\,\boldsymbol{\xi}_\mu, \tag{B4}$$

where $(l,1,j\,|\,m-\mu,\mu,m)$ are *Clebsh-Gordon coefficients* and $Y_{lm}(\theta,\varphi)$ are *spherical functions* defined according to [70] (see p. 119, Eqs. (28,7)–(28,8)). From Eq. (B2) one can obtain such a formula (at $\boldsymbol{\varepsilon}^{(3)}=0$):

$$e^{-i\alpha_i\mathbf{k}_\gamma\mathbf{r}}=\frac{1}{2}\sum_{\mu=\pm1}\boldsymbol{\xi}_\mu\,\mu\,\sqrt{2\pi}\sum_{l_\gamma=1}(2l_\gamma+1)^{1/2}\,(-i)^{l_\gamma}\;\cdot[\mathbf{A}^*_{l_\gamma\mu}(\mathbf{r},M)-i\mu\,\mathbf{A}^*_{l_\gamma\mu}(\mathbf{r},E)]. \tag{B5}$$

b. Central interactions

Using (B5), for (B1) we find

$$\langle\phi_f|\,e^{-i\alpha_i\mathbf{k}_\gamma\mathbf{r}}\,|\,\phi_i\rangle_{\mathbf{r}}=\sqrt{\frac{\pi}{2}}\sum_{l_\gamma=1}(-i)^{l_\gamma}\sqrt{2l_\gamma+1}\sum_{\mu=\pm1}\big[\mu\,\tilde{p}^M_{l_\gamma\mu}-i\,\tilde{p}^E_{l_\gamma\mu}\big],$$
$$\left\langle\phi_f\left|\,e^{-i\alpha_i\mathbf{k}_\gamma\mathbf{r}}\frac{\partial}{\partial\mathbf{r}}\,\right|\phi_i\right\rangle_{\mathbf{r}}=\sqrt{\frac{\pi}{2}}\sum_{l_\gamma=1}(-i)^{l_\gamma}\sqrt{2l_\gamma+1}\sum_{\mu=\pm1}\boldsymbol{\xi}_\mu\,\mu\,\times\big[p^M_{l_\gamma\mu}-i\mu\,p^E_{l_\gamma\mu}\big], \tag{B6}$$

where

$$p^M_{l_\gamma\mu}=\int\phi^*_f(\mathbf{r})\left(\frac{\partial}{\partial\mathbf{r}}\,\phi_i(\mathbf{r})\right)\mathbf{A}^*_{l_\gamma\mu}(\mathbf{r},M)\,\mathbf{dr},\quad p^E_{l_\gamma\mu}=\int\phi^*_f(\mathbf{r})\left(\frac{\partial}{\partial\mathbf{r}}\,\phi_i(\mathbf{r})\right)\mathbf{A}^*_{l_\gamma\mu}(\mathbf{r},E)\,\mathbf{dr} \tag{B7}$$

and

$$\tilde{p}^M_{l_\gamma\mu}=\boldsymbol{\xi}_\mu\int\phi^*_f(\mathbf{r})\,\phi_i(\mathbf{r})\,\mathbf{A}^*_{l_\gamma\mu}(\mathbf{r},M)\,\mathbf{dr},\quad \tilde{p}^E_{l_\gamma\mu}=\boldsymbol{\xi}_\mu\int\phi^*_f(\mathbf{r})\,\phi_i(\mathbf{r})\,\mathbf{A}^*_{l_\gamma\mu}(\mathbf{r},E)\,\mathbf{dr}. \tag{B8}$$

c. Calculations of the components $p^M_{l_\gamma\mu}$, $p^E_{l_\gamma\mu}$ and $\tilde{p}^M_{l_\gamma\mu}$, $\tilde{p}^E_{l_\gamma\mu}$

For calculation of these components we shall use the *gradient formula* (see [58], Eq. (2.56) on p. 46),

$$\frac{\partial}{\partial\mathbf{r}}\,\phi_i(\mathbf{r})=\frac{\partial}{\partial\mathbf{r}}\,\{R_i(r)\,Y_{l_im_i}(\widehat{\mathbf{r}})\}=\sqrt{\frac{l_i}{2l_i+1}}\left(\frac{dR_i(r)}{dr}+\frac{l_i+1}{r}\,R_i(r)\right)\mathbf{T}_{l_il_i-1,m_i}(\widehat{\mathbf{r}})$$
$$-\sqrt{\frac{l_i+1}{2l_i+1}}\left(\frac{dR_i(r)}{dr}-\frac{l_i}{r}\,R_i(r)\right)\mathbf{T}_{l_il_i+1,m_i}(\widehat{\mathbf{r}}), \tag{B9}$$

and obtain

$$p^M_{l_{\mathrm{ph},\mu}}=\sqrt{\frac{l_i}{2l_i+1}}\,I_M(l_i,l_f,l_\gamma,l_i-1,\mu)\{J_1(l_i,l_f,l_\gamma,\alpha_i)+(l_i+1)J_2(l_i,l_f,l_\gamma,\alpha_i)\}$$
$$-\sqrt{\frac{l_i+1}{2l_i+1}}\,I_M(l_i,l_f,l_\gamma,l_i+1,\mu)\{J_1(l_i,l_f,l_\gamma,\alpha_i)-l_iJ_2(l_i,l_f,l_\gamma,\alpha_i)\},$$

$$
\begin{aligned}
p^{E}_{l_{\mathrm{ph}},\mu} = & \sqrt{\frac{l_i\,(l_\gamma+1)}{(2l_i+1)(2l_\gamma+1)}}\,I_E(l_i,l_f,l_\gamma,l_i-1,l_\gamma-1,\mu)\{J_1(l_i,l_f,l_\gamma-1,\alpha_i)\ +(l_i+1)J_2(l_i,l_f,l_\gamma-1,\alpha_i)\}\\
& -\sqrt{\frac{l_i\,l_\gamma}{(2l_i+1)(2l_\gamma+1)}}\,I_E(l_i,l_f,l_\gamma,l_i-1,l_\gamma+1,\mu)\{J_1(l_i,l_f,l_\gamma+1,\alpha_i)\ +(l_i+1)J_2(l_i,l_f,l_\gamma+1,\alpha_i)\}\\
& +\sqrt{\frac{(l_i+1)(l_\gamma+1)}{(2l_i+1)(2l_\gamma+1)}}\,I_E(l_i,l_f,l_\gamma,l_i+1,l_\gamma-1,\mu)\{J_1(l_i,l_f,l_\gamma-1,\alpha_i)\ -l_iJ_2(l_i,l_f,l_\gamma-1,\alpha_i)\}\\
& -\sqrt{\frac{(l_i+1)\,l_\gamma}{(2l_i+1)(2l_\gamma+1)}}\,I_E(l_i,l_f,l_\gamma,l_i+1,l_\gamma+1,\mu)\{J_1(l_i,l_f,l_\gamma+1,\alpha_i)\ -l_iJ_2(l_i,l_f,l_\gamma+1,\alpha_i)\},
\end{aligned}
\tag{B10}
$$

where

$$
\begin{aligned}
J_1(l_i,l_f,n,\alpha_i) &= \int_0^{+\infty}\frac{dR_i(r,l_i)}{dr}\,R^*_f(l_f,r)\,j_n(\alpha_i\,k_\gamma r)\,r^2dr,\\
J_2(l_i,l_f,n,\alpha_i) &= \int_0^{+\infty}R_i(r,l_i)\,R^*_f(l_f,r)\,j_n(\alpha_i\,k_\gamma r)\,r\,dr,\\
I_M\,(l_i,l_f,l_\gamma,l_1,\mu) &= \int Y^*_{l_fm_f}(\widehat{\mathbf{r}})\,\mathbf{T}_{l_i\,l_1,\,m_i}(\widehat{\mathbf{r}})\,\mathbf{T}^*_{l_\gamma\,l_\gamma,\,\mu}(\widehat{\mathbf{r}})\,d\Omega,\\
I_E\,(l_i,l_f,l_\gamma,l_1,l_2,\mu) &= \int Y^*_{l_fm_f}(\widehat{\mathbf{r}})\,\mathbf{T}_{l_il_1,\,m_i}(\widehat{\mathbf{r}})\,\mathbf{T}^*_{l_\gamma l_2,\,\mu}(\widehat{\mathbf{r}})\,d\Omega.
\end{aligned}
\tag{B11}
$$

In the same way, for $\tilde{p}^{M}_{l_\gamma\mu}\ \tilde{p}^{E}_{l_\gamma\mu}$ we find

$$
\begin{aligned}
&\tilde{p}^{M}_{l_\gamma\mu} = \tilde{I}\,(l_i,l_f,l_\gamma,l_\gamma,\mu)\tilde{J}\,(l_i,l_f,l_\gamma,\alpha_i),\\
&\tilde{p}^{E}_{l_\gamma\mu} = \sqrt{\frac{l_\gamma+1}{2l_\gamma+1}}\,\tilde{I}\,(l_i,l_f,l_\gamma,l_\gamma-1,\mu)\tilde{J}\,(l_i,l_f,l_\gamma-1,\alpha_i) - \sqrt{\frac{l_\gamma}{2l_\gamma+1}}\,\tilde{I}\,(l_i,l_f,l_\gamma,l_\gamma+1,\mu)\tilde{J}\,(l_i,l_f,l_\gamma+1,\alpha_i),
\end{aligned}
\tag{B12}
$$

where

$$
\begin{aligned}
\tilde{J}\,(l_i,l_f,n,\alpha_i) &= \int_0^{+\infty}R_i(r)\,R^*_f(l,r)\,j_n(\alpha_i\,k_\gamma r)\,r^2dr,\\
\tilde{I}\,(l_i,l_f,l_\gamma,n,\mu) &= \boldsymbol{\xi}_\mu\int Y_{l_im_i}(\widehat{\mathbf{r}})\,Y^*_{l_fm_f}(\widehat{\mathbf{r}})\,\mathbf{T}^*_{l_\gamma n,\mu}(\widehat{\mathbf{r}})\,d\Omega.
\end{aligned}
\tag{B13}
$$

APPENDIX C: LINEAR AND CIRCULAR POLARIZATIONS OF THE EMITTED PHOTON

We define *vectors of linear polarization* of the emitted photon as (in Coulomb gauge at $\boldsymbol{\varepsilon}^{(3)}=0$):

$$
\boldsymbol{\varepsilon}^{(1)} = \frac{1}{\sqrt{2}}\,(\boldsymbol{\xi}_{-1}-\boldsymbol{\xi}_{+1}),\qquad \boldsymbol{\varepsilon}^{(2)} = \frac{i}{\sqrt{2}}\,(\boldsymbol{\xi}_{-1}+\boldsymbol{\xi}_{+1}),
\tag{C1}
$$

where $\boldsymbol{\xi}_\mu$ are *vectors of circular polarization* with opposite directions of rotation for the emitted photon used in Eqs. (B2). We rewrite vectors of linear polarization $\boldsymbol{\varepsilon}^{(\alpha)}$ through vectors of circular polarization $\boldsymbol{\xi}_\mu$ (see Ref. [58], Eq, (2.39), p. 42, and Appendix A in Ref. [5]; $\boldsymbol{\varepsilon}^{(\alpha),*}=\boldsymbol{\varepsilon}^{(\alpha)}$):

$$
\boldsymbol{\xi}_{-1} = \frac{1}{\sqrt{2}}(\boldsymbol{\varepsilon}^{(1)}-i\boldsymbol{\varepsilon}^{(2)}),\quad \boldsymbol{\xi}_{+1} = -\frac{1}{\sqrt{2}}(\boldsymbol{\varepsilon}^{(1)}+i\boldsymbol{\varepsilon}^{(2)}),\quad \boldsymbol{\xi}_0=\boldsymbol{\varepsilon}^{(3)}.
\tag{C2}
$$

We obtain properties

$$
\sum_{\alpha=1,2}\boldsymbol{\varepsilon}^{(\alpha),*} = h_{-1}\boldsymbol{\xi}^*_{-1}+h_{+1}\boldsymbol{\xi}^*_{+1},
\tag{C3}
$$

$$
\sum_{\mu=\pm1}\boldsymbol{\xi}^*_\mu\cdot\boldsymbol{\xi}_\mu = \frac{1}{2}\,(\boldsymbol{\varepsilon}^{(1)}-i\boldsymbol{\varepsilon}^{(2)})\,(\boldsymbol{\varepsilon}^{(1)}-i\boldsymbol{\varepsilon}^{(2)})^* + \frac{1}{2}\,(\boldsymbol{\varepsilon}^{(1)}+i\boldsymbol{\varepsilon}^{(2)})(\boldsymbol{\varepsilon}^{(1)}+i\boldsymbol{\varepsilon}^{(2)})^* = 2,
\tag{C4}
$$

where

$$h_{-1} = \frac{1}{\sqrt{2}}(1-i), \quad h_1 = -\frac{1}{\sqrt{2}}(1+i), \quad h_{-1} + h_1 = -i\sqrt{2}. \tag{C5}$$

Also there is property the (see Eqs. (3) and (5) in Ref. [71]):

$$\sum_{\alpha=1,2} \boldsymbol{\varepsilon}^{(\alpha),*} = \sum_{\mu=\pm1} h_m \, \boldsymbol{\xi}^*_m. \tag{C6}$$

We shall find multiplications of vectors $\boldsymbol{\xi}_{\pm1}$. From Eq. (C2) we obtain

$$\boldsymbol{\xi}^*_{-1} = \left(\frac{1}{\sqrt{2}}(\boldsymbol{\varepsilon}^{(1)} - i\boldsymbol{\varepsilon}^{(2)})\right)^* = \frac{1}{\sqrt{2}}(\boldsymbol{\varepsilon}^{(1)} + i\boldsymbol{\varepsilon}^{(2)}) = -\boldsymbol{\xi}_{+1}, \boldsymbol{\xi}^*_{+1} = -\boldsymbol{\xi}_{-1} \tag{C7}$$

and

$$\boldsymbol{\xi}^*_{-1} = -\boldsymbol{\xi}_{+1}, \quad \boldsymbol{\xi}^*_{+1} = -\boldsymbol{\xi}_{-1}. \tag{C8}$$

We check orthogonality conditions as

$$\begin{aligned} &\boldsymbol{\xi}_{-1}\cdot\boldsymbol{\xi}_{-1} = \boldsymbol{\xi}_{+1}\cdot\boldsymbol{\xi}_{+1} = 0, \quad \boldsymbol{\xi}_{-1}\cdot\boldsymbol{\xi}^*_{-1} = \boldsymbol{\xi}_{+1}\cdot\boldsymbol{\xi}^*_{+1} = -1, \\ &\boldsymbol{\xi}_{-1}\cdot\boldsymbol{\xi}_{+1} = 1, \quad \boldsymbol{\xi}_{-1}\cdot\boldsymbol{\xi}^*_{+1} = \boldsymbol{\xi}_{+1}\cdot\boldsymbol{\xi}^*_{-1} = 0. \end{aligned} \tag{C9}$$

We calculate multiplications of vectors as

$$\begin{aligned} &[\boldsymbol{\xi}^*_{-1}\times\boldsymbol{\xi}_{+1}] = -[\boldsymbol{\xi}_{+1}\times\boldsymbol{\xi}_{+1}] = 0, \quad [\boldsymbol{\xi}^*_{-1}\times\boldsymbol{\xi}_{-1}] = -[\boldsymbol{\xi}_{+1}\times\boldsymbol{\xi}_{-1}], \\ &[\boldsymbol{\xi}^*_{+1}\times\boldsymbol{\xi}_{-1}] = -[\boldsymbol{\xi}_{-1}\times\boldsymbol{\xi}_{-1}] = 0, \quad [\boldsymbol{\xi}^*_{+1}\times\boldsymbol{\xi}_{+1}] = -[\boldsymbol{\xi}_{-1}\times\boldsymbol{\xi}_{+1}], \end{aligned} \tag{C10}$$

and

$$[\boldsymbol{\xi}_{-1}\times\boldsymbol{\xi}^*_{-1}] = -[\boldsymbol{\xi}_{+1}\times\boldsymbol{\xi}^*_{+1}] = i[\boldsymbol{\varepsilon}^{(1)}\times\boldsymbol{\varepsilon}^{(2)}] = -[\boldsymbol{\xi}_{-1}\times\boldsymbol{\xi}_{+1}]. \tag{C11}$$

Now we take into account that two vectors $\boldsymbol{\varepsilon}^{(1)}$ and $\boldsymbol{\varepsilon}^{(2)}$ are vectors of polarization of the emitted photon which are perpendicular to the direction of emission of this photon defined by vector $\mathbf{k}$. The modulus of vectorial multiplication $[\boldsymbol{\varepsilon}^{(1)}\times\boldsymbol{\varepsilon}^{(2)}]$ equals unity. So, we have

$$[\boldsymbol{\varepsilon}^{(1)}\times\boldsymbol{\varepsilon}^{(2)}] = \frac{\mathbf{k}_\gamma}{|\mathbf{k}_\gamma|} \equiv \widehat{\gamma}. \tag{C12}$$

Using such a basis, we rewrite properties (C11) as

$$[\boldsymbol{\xi}_{-1}\times\boldsymbol{\xi}^*_{-1}] = -[\boldsymbol{\xi}_{+1}\times\boldsymbol{\xi}^*_{+1}] = -[\boldsymbol{\xi}_{-1}\times\boldsymbol{\xi}_{+1}] = i[\boldsymbol{\varepsilon}^1\times\boldsymbol{\varepsilon}^2] = i\,\widehat{\gamma}. \tag{C13}$$

APPENDIX D: ANGULAR INTEGRALS I_E, I_M, AND $\tilde{I}$

We shall calculate the integrals in Eqs. (B11) and (B13) (see Appendix B in Ref. [5]):

$$\begin{aligned} I_M(l_i,l_f,l_\gamma,l_1,\mu) &= \int Y^*_{l_f m_f}(\widehat{\mathbf{r}})\,\mathbf{T}_{l_i l_1, m_i}(\widehat{\mathbf{r}})\,\mathbf{T}^*_{l_\gamma l_\gamma,\mu}(\widehat{\mathbf{r}})\,d\Omega, \\ I_E(l_i,l_f,l_\gamma,l_1,l_2,\mu) &= \int Y^*_{l_f m_f}(\widehat{\mathbf{r}})\,\mathbf{T}_{l_i l_1, m_i}(\widehat{\mathbf{r}})\,\mathbf{T}^*_{l_\gamma l_2,\mu}(\widehat{\mathbf{r}})\,d\Omega, \\ \tilde{I}(l_i,l_f,l_\gamma,n,\mu) &= \xi_\mu \int Y^*_{l_f m_f}(\widehat{\mathbf{r}})\,Y_{l_i m_i}(\widehat{\mathbf{r}})\,\mathbf{T}^*_{l_\gamma n,\mu}(\widehat{\mathbf{r}})\,d\Omega. \end{aligned} \tag{D1}$$

Substituting the function $\mathbf{T}_{jl,m}(\widehat{\mathbf{r}})$ defined by Eq. (B4), we obtain (at $\xi_0 = 0$)

$$I_M(l_i,l_f,l_\gamma,l_1,\mu) = \sum_{\mu'=\pm1} (l_1,1,l_i\,|\,m_i-\mu',\mu',m_i)\,(l_\gamma,1,l_\gamma\,|\,\mu-\mu',\mu',\mu)\int Y^*_{l_f m}(\widehat{\mathbf{r}})\cdot Y_{l_1,m_i-\mu'}(\widehat{\mathbf{r}})\cdot Y^*_{l_\gamma,\mu-\mu'}(\widehat{\mathbf{r}})\,d\Omega,$$

$$I_E(l_i,l_f,l_\gamma,l_1,l_2,\mu) = \sum_{\mu'=\pm1} (l_1,1,l_i\,|\,m_i-\mu',\mu',m_i)\,(l_2,1,l_\gamma\,|\,\mu-\mu',\mu',\mu)\int Y^*_{l_f m}(\widehat{\mathbf{r}})\cdot Y_{l_1,m_i-\mu'}(\widehat{\mathbf{r}})\cdot Y^*_{l_2,\mu-\mu'}(\widehat{\mathbf{r}})\,d\Omega, \tag{D2}$$

$$\tilde{I}(l_i,l_f,l_\gamma,n,\mu) = (n,1,l_\gamma\,|\,0,\mu,\mu)\times\int Y^*_{l_f m_f}(\widehat{\mathbf{r}})\,Y_{l_i m_i}(\widehat{\mathbf{r}})\,Y^*_{n0}(\widehat{\mathbf{r}})\,d\Omega. \tag{D3}$$

Here, we have taken orthogonality of vectors $\xi_{\pm1}$ into account. In these formulas we shall find the angular integral

$$\int Y^*_{l_f m_f}(\widehat{\mathbf{r}})\, Y_{l_1,\, m_i-\mu'}(\widehat{\mathbf{r}})\, Y^*_{n,\,\mu-\mu'}(\widehat{\mathbf{r}})\, d\Omega = (-1)^{l_f+n+m_i-\mu'}\; i^{l_f+l_1+n+|m_f|+|m_i-\mu'|+|m_i-m_f-\mu'|}$$
$$\times \sqrt{\frac{(2l_f+1)\,(2l_1+1)\,(2n+1)}{16\pi}\,\frac{(l_f-|m_f|)!}{(l_f+|m_f|)!}\,\frac{(l_1-|m_i-\mu'|)!}{(l_1+|m_i-\mu'|)!}\,\frac{(n-|m_i-m_f-\mu'|)!}{(n+|m_i-m_f-\mu'|)!}}$$
$$\times \int_0^\pi P_{l_f}^{|m_f|}(\cos\theta)\, P_{l_1}^{|m_i-\mu'|}(\cos\theta)\, P_n^{|m_i-m_f-\mu'|}(\cos\theta)\sin\theta\, d\theta, \tag{D4}$$

where $P_l^m(\cos\theta)$ are associated Legandre polynomials, and we obtain the conditions

$$\text{for integrals } I_M, I_E : \mu = m_i - m_f, \quad n \geqslant |\mu-\mu'| = |m_i - m_f + \mu'|, \quad \mu = \pm 1,$$
$$\text{for integral } \tilde{I} : m_i = m_f. \tag{D5}$$

Using formula (D4), we calculate integrals (D2) and (D3):

$$I_M\,(l_i, l_f, l_\gamma, l_1, \mu) = \delta_{\mu,m_i-m_f} \sum_{\mu'=\pm1} C^{m_i m_f \mu'}_{l_i l_f l_{ph} l_1 l_{ph}} \int_0^\pi f^{m_i m_f \mu'}_{l_1 l_f l_\gamma}(\theta)\sin\theta\, d\theta,$$
$$I_E\,(l_i, l_f, l_\gamma, l_1, l_2, \mu) = \delta_{\mu,m_i-m_f} \sum_{\mu'=\pm1} C^{m_i m_f \mu'}_{l_i l_f l_{ph} l_1 l_2} \int_0^\pi f^{m_i m_f \mu'}_{l_1 l_f l_2}(\theta)\sin\theta\, d\theta,$$
$$\tilde{I}\,(l_i, l_f, l_\gamma, n, \mu) = C^{m_i \mu}_{l_i l_f l_\gamma n} \int_0^\pi f^{m_i m_i 0}_{l_i l_f n}(\theta)\sin\theta\, d\theta, \tag{D6}$$

where

$$C^{m_i m_f \mu'}_{l_i l_f l_{ph} l_1 l_2} = (-1)^{l_f+l_2+m_i-\mu'}\; i^{l_f+l_1+l_2+|m_f|+|m_i-\mu'|+|m_i-m_f-\mu'|}$$
$$\times\,(l_1, 1, l_i \,|\, m_i-\mu', \mu', m_i)\;(l_2, 1, l_\gamma \,|\, m_i-m_f-\mu', \mu', m_i-m_f)$$
$$\times \sqrt{\frac{(2l_f+1)\,(2l_1+1)\,(2l_2+1)}{16\pi}\,\frac{(l_f-|m_f|)!}{(l_f+|m_f|)!}\,\frac{(l_1-|m_i-\mu'|)!}{(l_1+|m_i-\mu'|)!}\,\frac{(l_2-|m_i-m_f-\mu'|)!}{(l_2+|m_i-m_f-\mu'|)!}}, \tag{D7}$$

$$C^{m_i\mu}_{l_i l_f l_\gamma n} = (-1)^{l_f+n+m_i+|m_i|}\; i^{l_f+l_i+n}\cdot(n, 1, l_\gamma \,|\, 0, \mu, \mu)\cdot\sqrt{\frac{(2l_f+1)\,(2l_i+1)\,(2n+1)}{16\pi}\,\frac{(l_f-|m_i|)!}{(l_f+|m_i|)!}\,\frac{(l_i-|m_i|)!}{(l_i+|m_i|)!}}, \tag{D8}$$

$$f^{m_i m_f \mu'}_{l_1 l_f l_2}(\theta) = P_{l_1}^{|m_i-\mu'|}(\cos\theta)\, P_{l_f}^{|m_f|}(\cos\theta)\, P_{l_2}^{|m_i-m_f-\mu'|}(\cos\theta). \tag{D9}$$

We define differential functions on the integrals (D6) with angular dependence as

$$\frac{d\,I_M\,(l_i, l_f, l_\gamma, l_1, \mu)}{\sin\theta\, d\theta} = \delta_{\mu,m_i-m_f} \sum_{\mu'=\pm1} C^{m_i m_f \mu'}_{l_i l_f l_{ph} l_1 l_{ph}} f^{m_i m_f \mu'}_{l_1 l_f l_\gamma}(\theta),$$
$$\frac{d\,I_E\,(l_i, l_f, l_\gamma, l_1, l_2, \mu)}{\sin\theta\, d\theta} = \delta_{\mu,m_i-m_f} \sum_{\mu'=\pm1} C^{m_i m_f \mu'}_{l_i l_f l_{ph} l_1 l_2} f^{m_i m_f \mu'}_{l_1 l_f l_2}(\theta),$$
$$\frac{d\,\tilde{I}\,(l_i, l_f, l_\gamma, n, \mu)}{\sin\theta\, d\theta} = \delta_{m_i m_f}\, C^{m_i\mu}_{l_i l_f l_\gamma n} f^{m_i m_i 0}_{l_i l_f n}(\theta). \tag{D10}$$

APPENDIX E: CALCULATIONS OF THE WAVE FUNCTIONS OF RELATIVE MOTION BETWEEN TWO NUCLEI

1. Boundary conditions and normalization of the wave functions

In this paper, for the wave function of relative motion $\phi(\mathbf{r})$ in the initial state i and final state f we chose states of the elastic scattering of one nucleus on another nucleus, for which we have used the normalization condition for the radial wave function of relative motion, $R_s(k, r)$, as (see Ref. [70], p. 138)

$$\int_0^{+\infty} R^*_s(k', r)\, R_s(k, r)\, r^2 dr = \int_0^{+\infty} \chi^*_s(k', r)\, \chi_s(k, r)\, dr = 2\pi\,\delta(k'-k), \quad R_s(k, r) = \frac{\chi_s(k, r)}{r}. \tag{E1}$$

Here, r is relative distance between nuclei and k, k' are wave numbers. The radial wave function in the asymptotic region can be written as ($s = i, f$)

$$\chi_s(k, r) = N_s[A_s G_s(k, r) + B_s F_s(k, r)], \tag{E2}$$

where F_s and G_s are the Coulomb functions, A_s and B_s are real constants determined concerning the found solution for $\chi_s(k, r)$ at small r, and N_s is an unknown normalization factor. At far distances we have

$$F_s(k, r) = \sin\theta_s,\ \ G_s(k, r) = \cos\theta_s,\ \ \theta_s = k_s r - \frac{l\pi}{2} + \sigma_l(\eta_s), \tag{E3}$$

where $\sigma_l(\eta_s) = \arg\,\Gamma(i\eta_s + l + 1)$, $\eta_s = \frac{\mu\, m_N\, \nu}{k_s\, \hbar}$, $\nu = Z_1\, Z_2\, e^2$ is Coulomb parameter, $\mu\, m_N = m_1 m_2/(m_1 + m_2)$ is the reduced mass of two nuclei with mass m_1 and m_2, and e is the electric charge of a proton. With such a representation of the asymptotic Coulomb functions we find

$$\begin{aligned}(A_s G_s(k', r) + B_s F_s(k', r))^*(A_s G_s(k, r) + B_s F_s(k, r)) \\ = \frac{A_s^2 + B_s^2}{2}\cos(\theta' + \theta) + A_s B_s \sin(\theta' + \theta) \\ + \frac{A_s^2 + B_s^2}{2}\cos(\theta' - \theta).\end{aligned} \tag{E4}$$

On such a basis, the integral (E1) is transformed to the following form:

$$|N_s|^2 \frac{A_s^2 + B_s^2}{2}\int_0^{+\infty}\cos(\theta' - \theta)\, dr = 2\pi\ \delta(k' - k). \tag{E5}$$

Taking the definition of the δ function into account, we obtain

$$N_s = \frac{2}{\sqrt{A_s^2 + B_s^2}}. \tag{E6}$$

In bremsstrahlung problems another normalization condition is useful for decay of nuclear system, so we add this formalism. The wave function should correspond to emission of a cluster from a nucleus during a unit of time (see Ref. [70], p. 140):

$$\oint j_s(\mathbf{r})\, r^2\, d\Omega = 1, \quad \chi_s(r \to +\infty) = N_s[G_s(r) + iF_s(r)], \tag{E7}$$

where $d\Omega = \sin\theta\, d\theta\, d\phi$ is the solid angle element, $j_s(\mathbf{r})$ is the probability flux density, and the integration is performed over a spherical surface of enough large radius, $R_{\max}$. We define the flux as $j_s(\mathrm{r}) = i/2m\,[\phi_s(\mathbf{r})\,\nabla\phi_s^*(\mathbf{r}) - \mathrm{c.c.}]$ and choose the radial component, $\chi_s(r)$, at far distances as the outgoing Coulomb wave [see second formula in Eqs. (E7)], where N_s is an unknown normalization factor. We integrate Eq. (E7) over the angular variables and find N_s as

$$\begin{aligned}\left(\frac{k_s}{m}|\chi_s(R_{\max})|^2 = \frac{k_s}{m}\,|N_s|^2(|G_s(R_{\max})|^2 + |F_s(R_{\max})|^2)\right. \\ \left. = \frac{k_s}{m}|N_s|^2 = 1\right) \to \left(N_s = \sqrt{\frac{m}{k_s}}\right).\end{aligned} \tag{E8}$$

2. Aspects of numerical calculations of the wave functions

To calculate integrals (B11) and (B13), we used a large but finite range for the variable r: $0 \leqslant r \leqslant R_{\max}$. We separate the full radial region into the internal and asymptotic parts at point R_{at}: the internal region with strong effects of nuclear and Coulomb interactions between clusters ($0 \leqslant r \leqslant R_{at}$), and the asymptotic region with the Coulomb interaction only ($R_{\mathrm{at}} \leqslant r \leqslant R_{\max}$). Calculations of the wave functions are performed in each region independently by different methods.

In the internal region we use the following method. For the state of elastic scattering the wave function, χ_s, is real. We determine each partial solution of the wave function and its derivative at a selected starting point r_0, and then we calculate those in the region close enough to this point using the *method of beginning of the solution* (based on expansion in Taylor series; see Ref. [72]). For the solution increasing in the barrier region we choose $r_0 = 0$ as the starting point. For the solution decreasing in the barrier region we choose $r_0 = R_{\mathrm{at}}$ as the starting point. Then we calculate both partial solutions and their derivatives independently in the full nuclear region using the *method of continuation of the solution* briefly presented in Appendix B.3 in Ref. [73], which is an improvement of the Numerov method with constant step [72]. Then, we find the unknown complex coefficients from the corresponding boundary conditions.

The Coulomb wave functions and their derivatives in the asymptotic region are calculated by using library programs. Then, they are matched at point R_{at} with the solutions in the internal region, using continuity conditions for the wave functions and their derivatives. The $R_{\max}$ boundary is chosen with requirement to achieve convenient stability and convergence in the calculations of the cross sections (this can be boundary of about 200 000 fm).

[1] M. Ya. Amusia, "Atomic" bremsstrahlung, Phys. Rep. **162**, 249 (1988).
[2] V. A. Pluyko and V. A. Poyarkov, Bremsstrahlung in reactions induced by protons, Phys. El. Part. At. Nucl. **18**, 374 (1987).
[3] V. V. Kamanin, A. Kugler, Yu. E. Penionzhkevich, I. S. Batkin, and I. V. Kopytin, High-energy gamma-ray emission in heavyion reactions at nonrelativistic energies, Phys. Elem. Part. At. Nucl. **20**, 743 (1989).
[4] C. A. Bertulani and G. Baur, Electromagnetic processes in relatevistic heavy ion collisions, Phys. Rep. **163**, 299 (1988).
[5] S. P. Maydanyuk, Model for bremsstrahlung emission accompanying interactions between protons and nuclei from low energies up to intermediate energies: Role of magnetic emission, Phys. Rev. C **86**, 014618 (2012).
[6] S. P. Maydanyuk and P.-M. Zhang, New approach to determine proton-nucleus interactions from experimental

bremsstrahlung data, Phys. Rev. C **91**, 024605 (2015).
[7] X. Liu, S. P. Maydanyuk, P.-M. Zhang, and L. Liu, First investigation of hypernuclei in reactions via analysis of emitted bremsstrahlung photons, Phys. Rev. C **99**, 064614 (2019).
[8] M. J. van Goethem, L. Aphecetche, J. C. S. Bacelar, H. Delagrange, J. Diaz, D. d'Enterria, M. Hoefman, R. Holzmann, H. Huisman, N. Kalantar-Nayestanaki, A. Kugler, H. Löhner, G. Martinez, J. G. Messchendorp, R. W. Ostendorf, S. Schadmand, R. H. Siemssen, R. S. Simon, Y. Schutz, R. Turrisi, M. Volkerts *et al.* Suppresion of soft nuclear bremsstrahlung in proton-nucleus collisions, Phys. Rev. Lett. **88**, 122302 (2002).
[9] D. Baye and P. Descouvemont, Microscopic description of nucleus-nucleus bremsstrahlung, Nucl. Phys. A **443**, 302 (1985).
[10] Q. K. K. Liu, Y. C. Tang, and H. Kanada, Microscopic calculation of bremsstrahlung emission in ^{3}He + α collisions, Phys. Rev. C **41**, 1401 (1990).
[11] Q. K. K. Liu, Y. C. Tang, and H. Kanada, Microscopic study of $p + \alpha$ bremsstrahlung, Phys. Rev. C **42**, 1895 (1990).
[12] D. Baye, C. Sauwens, P. Descouvemont, and S. Keller, Accurate treatment of Coulomb contribution in nucleus-nucleus bremsstrahlung, Nucl. Phys. A **529**, 467 (1991).
[13] Q. K. K. Liu, Y. C. Tang, and H. Kanada, Approximate treatment of antisymmetrization in the microscopic studies of $p + \alpha$ and ^{3}He + α bremsstrahlung, Phys. Rev. C **44**, 1695 (1991).
[14] D. Baye, P. Descouvemont, and M. Kruglanski, Probing scattering wave functions with nucleus-nucleus bremsstrahlung, Nucl. Phys. A **550**, 250 (1992).
[15] Q. K. K. Liu, Y. C. Tang, and H. Kanada, Microscopic study of $\alpha + \alpha$ bremsstrahlung with resonating-group wave functions, Few-Body Syst. **12**, 175 (1992).
[16] M. Kruglanski, D. Baye, and P. Descouvemont, Alpha-alpha bremsstrahlung in a microscopic model, in *Nuclei in the Cosmos 2*, edited by F. Kaeppeler and K. Wisshak (CRC, Boca Raton, 1993), pp. 423–428.
[17] J. Dohet-Eraly and D. Baye, Siegert approach within a microscopic description of nucleus-nucleus bremsstrahlung Phys. Rev. C **88**, 024602 (2013).
[18] J. Dohet-Eraly, D. Baye, and P. Descouvemont, Microscopic description of $\alpha + \alpha$ bremsstrahlung from a realistic nucleon-nucleon interaction J. Phys.: Conf. Ser. **436**, 012030 (2013).
[19] J. Dohet-Eraly, Microscopic cluster model of elastic scattering and bremsstrahlung of light nuclei, Ph.D. thesis, Universite Libre De Bruxelles, 2013 (unpublished).
[20] J. Dohet-Eraly, Microscopic description of $\alpha + N$ bremsstrahlung by a Siegert approach, Phys. Rev. C **89**, 024617 (2014).
[21] J. Dohet-Eraly and D. Baye, Comparison of potential models of nucleus-nucleus bremsstrahlung, Phys. Rev. C **90**, 034611 (2014).
[22] D. Baye, Extension of the Siegert theorem for photon emission, Phys. Rev. C **86**, 034306 (2012).
[23] J. A. Edgington and B. Rose, Nuclear bremsstrahlung from 140 MeV protons, Nucl. Phys. **89**, 523 (1966).
[24] P. F. M. Koehler, K. W. Rothe, and E. H. Thorndike, Neutron-proton bremsstrahlung at 197 MeV, Phys. Rev. Lett. **18**, 933 (1967).
[25] M. K. Njock, M. Maurel, H. Nifenecker, J. Pinston, F. Schussler, D. Barneoud, S. Drissi, J. Kern, and J. P. Vorlet, Nuclear bremsstrahlung production in proton-nucleus reactions at 72 MeV, Phys. Lett. B **207**, 269 (1988).
[26] J. A. Pinston, D. Barneoud, V. Bellini, S. Drissi, J. Guillot, J. Julien, M. Kwato Njock, H. Nifenecker, M. Maurel, F. Schussler, and J. P. Vorlet, Nuclear bremsstrahlung production in proton-nucleus reactions at 168 and 200 MeV, Phys. Lett. B **218**, 128 (1989).
[27] J. A. Pinston, D. Barneoud, V. Bellini, S. Drissi, J. Guillot, J. Julien, H. Nifenecker, and F. Schussler, Proton-deuterium bremsstrahlung at 200 MeV, Phys. Lett. B **249**, 402 (1990).
[28] H. Boie, H. Scheit, U. D. Jentschura, F. Köck, M. Lauer, A. I. Milstein, I. S. Terekhov, and D. Schwalm, Bremsstrahlung in α decay reexamined, Phys. Rev. Lett. **99**, 022505 (2007).
[29] H. Boie, Bremsstrahlung emission probability in the α decay of ^{210}Po, Ph.D. thesis, Ruperto-Carola University of Heidelberg, Germany, 2009 (unpublished).
[30] A. D'Arrigo, N. V. Eremin, G. Fazio, G. Giardina, M. G. Glotova, T. V. Klochko, M. Sacchi, and A. Taccone, Investigation of bremsstrahlung emission in α-decay of heavy nuclei, Phys. Lett. B **332**, 25 (1994).
[31] J. Kasagi, H. Yamazaki, N. Kasajima, T. Ohtsuki, and H. Yuki, Bremsstrahlung emission in α decay and tunneling motion of α particle, J. Phys. G **23**, 1451 (1997).
[32] J. Kasagi, H. Yamazaki, N. Kasajima, T. Ohtsuki, and H. Yuki, Bremsstrahlung in α decay of ^{210}Po: Do α particles emit photons in tunneling? Phys. Rev. Lett. **79**, 371 (1997).
[33] G. Giardina, G. Fazio, G. Mandaglio, M. Manganaro, C. Saccá, N. V. Eremin, A. A. Paskhalov, D. A. Smirnov, S. P. Maydanyuk, and V. S. Olkhovsky, Bremsstrahlung emission accompanying alpha-decay of ^{214}Po, Eur. Phys. J. A **36**, 31 (2008).
[34] G. Giardina, G. Fazio, G. Mandaglio, M. Manganaro, S. P. Maydanyuk, V. S. Olkhovsky, N. V. Eremin, A. A. Paskhalov, D. A. Smirnov, and C. Saccá, Bremsstrahlung emission during α decay of ^{226}Ra, Mod. Phys. Lett. A **23**, 2651 (2008).
[35] N. V. Eremin, A. A. Paskhalov, S. S. Markochev, E. A. Tsvetkov, G. Mandaglio, M. Manganaro, G. Fazio, G. Giardina, and M. V. Romaniuk, Int. J. Mod. Phys. E **19**, 1183 (2010).
[36] S. P. Maydanyuk, V. S. Olkhovsky, G. Mandaglio, M. Manganaro, G. Fazio, and G. Giardina, Bremsstrahlung emission of high energy accompanying spontaneous of ^{252}Cf, Phys. Rev. C **82**, 014602 (2010).
[37] H. van der Ploeg, J. C. S. Bacelar, A. Buda, C. R. Laurens, and A. van der Woude, Emission of photons in spontaneous fission of ^{252}Cf, Phys. Rev. C **52**, 1915 (1995).
[38] J. Kasagi, H. Hama, K. Yoschida, M. Sakurai, and K. Ishii, Nucleus-nucleus bremsstrahlung observed in the spontaneous fission of ^{252}Cf, Proc. Fifth Int. Conf. Clustering Aspects in Nucl. and Subnucl. Systems, Kyoto, 1988, J. Phys. Soc. Jpn. Suppl. **58**, 620 (1989).
[39] S. J. Luke, C. A. Gossett, and R. Vandenbosch, Search for high energy rays from the spontaneous fission of ^{252}Cf, Phys. Rev. C **44**, 1548 (1991).
[40] V. A. Varlachev, G. N. Dudkin, and V. N. Padalko, Study of the high-energy part of the spectrum of rays from the neutron-induced fission reaction of ^{235}U nuclei, Bull. Russ. Acad. Sci.: Phys. **71**, 1635 (2007).
[41] D. J. Hofman, B. B. Back, C. P. Montoya, S. Schadmand, R. Varma, and P. Paul, High energy rays from ^{252}Cf spontaneous fission, Phys. Rev. C **47**, 1103 (1993).

[42] D. Pandit, S. Mukhopadhyay, S. Bhattacharya, S. Pal, A. De, and S. R. Banerjee, Coherent bremsstrahlung and GDR width from ^{252}Cf cold fission, Phys. Lett. B **690**, 473 (2010).

[43] D. Pierroutsakou, B. Martin, G. Inglima, A. Boiano, A. De Rosa, M. Di Pietro, M. La Commara, R. Mordente, M. Romoli, M. Sandoli, M. Trotta, E. Vardaci, T. Glodariu, M. Mazzocco, C. Signorini, L. Stroe, V. Baran, M. Colonna, M. Di Toro, and N. Pellegriti, Evolution of the prompt dipole γ-ray emission with incident energy in fusion reactions, Phys. Rev. C **71**, 054605 (2005).

[44] B. Wasilewska, M. Kmiecik, M. Ciemała, A. Maj, J. Łukasik, P. Pawłowski, B. Sowicki, M. Zięębliński, J. Gręebosz, F. C. L. Crespi, P. Bednarczyk, A. Bracco, S. Brambilla, I. Ciepał, N. Cieplicka-Oryønczak, B. Fornal, K. Guguła, M. N. Harakeh, M. Jeżabek, M. Kiciønska-Habior, M. Krzysiek, P. Kulessa *et al.*, Measurement of the γ decay from the energy region of the pygmy dipole states excited in the ^{208}Pb$(p, p'\gamma)$ reaction at CCB, Acta Phys. Pol. B **51**, 677 (2020).

[45] E. G. Lanza, L. Pellegri, A. Vitturi, and M. V. Andrés, Theoretical studies of pygmy resonances, Prog. Part. Nucl. Phys. **129**, 104006 (2023).

[46] I. V. Kopitin, M. A. Dolgopolov, T. A. Churakova, and A. S. Kornev, Electromagnetic Radiation in Nucleon-Nucleus Collisions, Phys. At. Nucl. **60**, 776 (1997) [Rus. ed.: Yad. Fiz. **60**, 869 (1997)].

[47] R. G. Thomas, A formulation of the theory of alpha-particle decay from time-independent equations Prog. Theor. Phys. **12**, 253 (1954).

[48] D. S. Delion, A. Insolia, and R. J. Liotta, Alpha widths in deformed nuclei: microscopic approach, Phys. Rev. C **46**, 1346 (1992).

[49] C. Xu and Z. Ren, New deformed model of α-decay half-lives with a microscopic potential, Phys. Rev. C **73**, 041301(R) (2006).

[50] D. S. Delion and R. J. Liotta, Shell-model representation to describe α emission, Phys. Rev. C **87**, 041302(R) (2013).

[51] I. Silişteanu and A. I. Budaca, Structure and α decay properties of heaviest nuclei, At. Data Nucl. Data Tables **98**, 1096 (2012).

[52] M. Ivascu and I. Silisteanu, Cluster radioactivity half-lives, Phys. Elem. Part. At. Nucl. **21**, 1405 (1990) [Sov. J. Part. Nucl. **21**, 599 (1990)].

[53] R. G. Lovas *et al.*, Microscopic theory of cluster radioactivity, Phys. Rep. **294**, 265 (1998).

[54] P. E. Hodgson and E. Betak, Cluster emission, transfer and capture in nuclear reactions, Phys. Rep. **374**, 1 (2003).

[55] S. P. Maydanyuk, V. S. Olkhovsky, G. Mandaglio, M. Manganaro, G. Fazio, and G. Giardina, Bremsstrahlung emission of photons accompanying ternary fission of ^{252}Cf, J. Phys.: Conf. Ser. **282**, 012016 (2011).

[56] J. A. Wheeler, Molecular viewpoints in nuclear structure, Phys. Rev. **52**, 1083 (1937).

[57] J. A. Wheeler, On the mathematical description of light nuclei by the method of resonating group structure, Phys. Rev. **52**, 1107 (1937).

[58] J. M. Eisenberg and W. Greiner, *Mehanizmi vozbuzhdenia yadra. Electromagnitnoie i slaboie vzaimodeistviya*, Vol. 2 (Atomizdat, Moskva, 1973), p. 348 [in Russian; English edition: *Excitation Mechanisms of the Nucleus. Electromagnetic and Weak Interactions* (North-Holland, Amsterdam, 1970)].

[59] D. R. Thompson, M. LeMere, and Y. C. Tang, Systematic investigation of scattering problems with the resonating-group method, Nucl. Phys. A **286**, 53 (1977).

[60] I. Reichstein and Y. C. Tang, Study of $N + \alpha$ system with the resonating-group method, Nucl. Phys. A **158**, 529 (1970).

[61] J. Clayton, W. Benenson, M. Cronqvist, R. Fox, D. Krofcheck, R. Pfaff, T. Reposeur, J. D. Stevenson, J. S. Winfield, B. Young, M. F. Mohar, C. Bloch, and D. E. Fields, Proton-deuteron bremsstrahlung at 145 and 195 MeV, Phys. Rev. C **45**, 1810 (1992).

[62] V. Herrmann, J. Speth, and K. Nakayama, Nucleon-nucleon bremsstrahlung at intermediate energies, Phys. Rev. C **43**, 394 (1991).

[63] M. Hoefman, L. Aphecetche, J. C. S. Bacelar, H. Delagrange, P. Descouvemont, J. Diaz, D. d'Enterria, M.-J. van Goethem, R. Holzmann, H. Huisman, N. Kalantar-Nayestanaki, A. Kugler, H. Lohner, F. M. Marques, G. Martinez, J. G. Messchendorp, R. W. Ostendorf, S. Schadmand, R. H. Siemssen, R. S. Simon, Y. Schutz *et al.*, Coherent bremsstrahlung in the $\alpha + p$ system at 50 MeV/nucleon, Phys. Rev. Lett. **85**, 1404 (2000).

[64] M. Hoefman, H. W. Wilschut, L. Aphecetche, J. S. Bacelar, H. Delagrange, J. Diaz, M.-J. van Goethem, R. Holzmann, H. Huisman, N. Kalantar-Nayestanaki, A. Kugler, H. Lohner, G. Martinez, J. G. Messchendorp, R. W. Ostendorf, S. Schadmand, Y. Schutz, M. Seip, R. H. Siemssen, R. S. Simon *et al.*, Coherent bremsstrahlung in $\alpha + p$ reactions at 50 MeV/nucleon, Nucl. Phys. A **654**, 779c (1999).

[65] M. Hoefman, A study of coherent bremsstrahlung and radiative capture, Ph.D. thesis, University of Groningen/UMCG, 1999 (unpublished).

[66] Z. M. Ding, D. Lin, and M. K. Liou, Special two-energy-two-angle approximation for bremsstrahlung, Phys. Rev. C **40**, 1291 (1989).

[67] M. K. Liou, R. G. E. Timmermans, and B. F. Gibson, Novel soft photon analysis of $pp\gamma$ below pion production threshold, Phys. Lett. B **345**, 372 (1995).

[68] H. R. Weller, H. Hasan, S. Manglos, G. Mitev, N. R. Roberson, S. L. Blatt, H. J. Hausman, R. G. Seyler, R. N. Boyd, T. R. Donoghue, M. A. Kovash, A. D. Bacher, and C. C. Foster, Proton capture to bound and unbound states of ^{12}C, Phys. Rev. C **25**, 2921 (1982).

[69] A. I. Ahiezer and V. B. Berestetskii, *Kvantovaya Elektrodinamika* (Nauka, Moskva, 1981), p. 432 [in Russian].

[70] L. D. Landau and E. M. Lifshitz, *Kvantovaya Mehanika, kurs Teoreticheskoi Fiziki*, Vol. 3 (Nauka, Mockva, 1989), p. 768 [in Russian; English edition: *Quantum Mechanics, Course of Theoretical Physics* (Pergamon, Oxford, 1982)].

[71] S. P. Maydanyuk and V. S. Olkhovsky, Angular analysis of bremsstrahlung in α-decay, Eur. Phys. J. A **28**, 283 (2006).

[72] K. S. Kunz, *Chislenniy analis* (Tehnika, Kyiv, 1964) [in Russian; English edition: *Numerical Analysis* (McGraw-Hill, New York, 1957)].

[73] S. P. Maydanyuk, Multipolar model of bremsstrahlung accompanying proton decay of nuclei, J. Phys. G **38**, 085106 (2011).